THESIS FOR THE DEGREE OF LICENTIATE OF ENGINEERING

Study of bio-oil and bio-char production from thermal and catalytic hydrotreatment of simulated pyrolysis oil under mild conditions

Elham Nejadmoghadam

Institutionen för Kemi och Kemiteknik
Chalmers Tekniska Högskola
SE-41296 Göteborg
Telefon +46(0)31-772 1000

Chemical Engineering Division
Department of Chemistry and Chemical Engineering
CHALMERS UNIVERSITY OF TECHNOLOGY
Göteborg, Sweden 2023

Study of bio-oil and bio-char production from thermal and catalytic hydrotreatment of simulated pyrolysis oil under mild conditions
Elham Nejadmoghadam

Licentiatuppsatser vid Institutionen för kemi och kemiteknik
Chalmers tekniska högskola.
Nr 2023:01

Department of Chemistry and Chemical Engineering
Chalmers University of Technology
SE-412 96 Gothenburg
Sweden
Telephone + 46 (0)31-772 1000

Printed by Chalmers Digitaltryck
Gothenburg, Sweden 2023

Study of bio-oil and bio-char production from thermal and catalytic hydrotreatment of simulated pyrolysis oil under mild conditions

Elham Nejadmoghadam

Department of Chemistry and Chemical Engineering
Chalmers University of Technology, Gothenburg 2023

Abstract

Pyrolysis oil derived from fast pyrolysis of lignocellulosic biomass is a promising alternative energy source used to produce renewable biofuels. However, the high reactivity of unsaturated oxygenated compounds in pyrolysis oil results in charring and deactivation of the catalyst under severe hydrotreatment conditions. This thesis focuses on reactions during stabilization of such oils, specifically, the undesirable carbon loss to solid char as the main side reaction.

In the first study, mild thermal and catalytic hydrotreatment of a simulated pyrolysis oil, containing a comprehensive mixture of various oxygenated groups, was performed using $NiMo/Al_2O_3$ under mild conditions of 180-300°C and 60 bar hydrogen in a batch reactor. The solid products were extracted into soluble and insoluble solid fractions to determine the degree of polymerization. It was found that the soluble solids transformed into the bio-liquid product and solid insoluble yield was suppressed at elevated temperatures. It was also accompanied by a higher degree of hydrodeoxygenation (HDO) causing the stabilization of light oxygenates, and a significant decrease in the formation of heavy oligomers in the liquid phase. In catalyst-free experiments, the formation of solids was higher and showed a decreasing trend when increasing the temperature, except during heating where no solids were observed for the non-catalytic experiment. In the presence of the catalyst, the soluble solids at lower temperatures (180°C) consisted of macromolecule structures that were rich in sugar derivatives, while the corresponding insoluble solids were not fully developed into char. Their composition changed to aliphatic compounds and fully developed char respectively at higher temperatures. Moreover, the removal of furan and sugar compounds was found to be crucial to reduce the solid char formation.

In the second study, a set of catalysts; Pt/Al_2O_3, Rh/Al_2O_3, Pd/Al_2O_3, Re/Al_2O_3, and $NiMo\text{-}S/Al_2O_3$ was used to stabilize the same simulated pyrolysis oil at identical reaction conditions (180°C) as applied in the first study. The catalyst screening results showed that Pd/Al_2O_3 was significantly better in terms of achieving the highest conversion of pyrolysis oil and producing a high yield (66 wt%) of liquid oil product. The bio-liquid was mostly composed of low molecular weight compounds such as stabilized oxygenates and hydrocarbons. It also featured a minimum solid formation (3.3 wt%) in which soluble polymers were more pronounced. The results also indicated that $NiMo\text{-}S/Al_2O_3$ was fairly good in catalyzing reactive compounds, except furans, into stable light oxygenates with the formed solids rich in heavy insoluble polymers (13.6 wt%). The Rh/Al_2O_3 was comparable to $NiMo\text{-}S/Al_2O_3$, however, Pt/Al_2O_3 and particularly Re/Al_2O_3 rendered poor performances with the lowest yields and qualities of the liquid products, consisting mainly of heavy soluble oligomers, which resulted in a high degree of polymerization.

Keywords: Stabilization, simulated pyrolysis oil, catalytic hydrotreatment, alumina-supported catalyst, soluble solid, insoluble solid/char

Acknowledgements

This work was performed at the Department of Chemistry and Chemical Engineering and Competence Centre for Catalysis at Chalmers University of Technology, Göteborg, Sweden.

First and foremost, I would like to express my deep gratitude to Professor Derek Creaser and Professor Louise Olsson, my esteemed supervisors for providing me the chance to conduct my Ph.D. studies in their research group and an opportunity to work on a such fascinating project. I am thankful to you for all your continuous support, inspiration, patience, valuable comments, remarks, and engagement during this project. I am also thankful for your critics from experts' perspectives that helped to polish my thesis.

My sincere thanks also go to Dr. Abdenour Achour my co-supervisor for his generous support in lab work as well as constructive assistance and scientific ideas. You have given me valuable scientific input during the meetings and analysis of the results.

I would like to thank Preem AB as the industrial partner in this project. Many thanks to Dr. Olov Öhrman and Dr. Prakhar Arora for the feedback and our discussion from the industrial point of view during all project meetings.

Also, I thank Salam who has willingly shared his time for discussions and appreciate his guidance.

I would like to thank Michael Andersson-Sarning for his technical support during my experiments.

Furthermore, I would like to thank all my friends and colleagues at Chalmers University for their support on the way and for all the fun and wonderful moments. I am grateful to have you all during this journey.

Last but not the least, I would like to thank my lovely family for providing me with unfailing support. I am gratefully indebted to my parents Esfandiar and Irandokht who have always encouraged me to pursue my dreams.

Elham Nejadmoghadam

List of publications

I: Study of bio-oil and bio-char production from simulated pyrolysis oil under mild conditions using NiMo/Al_2O_3 catalyst

Elham Nejadmoghadam, Abdenour Achour, Pouya Sirous Rezaei, Muhammad Abdus Salam, Prakhar Arora, Olov Öhrman, Derek Creaser, and Louise Olsson

Submitted.

Contribution: I planned and defined the scope of the study with co-authors. I performed all experiments in this work. I analyzed the results with co-authors and wrote the manuscripts.

II: Stabilization of simulated pyrolysis oil by catalytic hydrotreatment using alumina-supported catalysts

Elham Nejadmoghadam, Abdenour Achour, Prakhar Arora, Olov Öhrman, Derek Creaser, and Louise Olsson

Manuscript

Contribution: I planned and defined the scope of the study with co-authors. I performed all experiments in this work. I analyzed the results with co-authors and wrote the manuscripts.

To my parents

List of abbreviations

APE Acetic acid, phenylmethyl ester

BET Brunauer Emmett Teller

BJH Barret Joyner Halenda

BMF Butanone, 4-(5-methyl-2-furanyl)-

CCM Cyclohexen-1-carboxaldehyde, 3-methyl-

DMSO Dimethyl sulfoxide

DMDS Dimethyl disulfide

DD 1,3-Dioxolane, 2,2-diethyl-

DMF Furan, 2,5-dimethyl-

DGG α-D-Glucopyranose, 4-O-β-D-galactopyranosyl-

FPBO fast pyrolysis bio-oil

FID Flame ionization detector

FPE Formic acid, phenylmethyl ester

FAT Furfuryl alcohol, tetrahydro-5-methyl-

FME Furan, 2,2'-methylenebis(5-methyl)

GC Gas chromatography

GHG Greenhouse gase

HDO Hydrodeoxygenation

HMF 5-hydroxymethylfurfural

HMP Hydroxy-2-(5-methylfuran-2-yl)1-phenylethanone

ICP-SFMS Inductively coupled plasma sector field mass spectrometry

LA Levulinic acid

LCB Lignocellulosic biomass

MF 5-methylfurfural

MFA 5-methyl furfuryl alcohol

MALDI Matrix Assisted Laser Desorption Ionization Time of Flight Mass Spectroscopy

ODT Oxetane, 2,4-dimethyl-, trans

RP R-(-)-1,2-propanediol

THFA Tetrahydrofurfuryl alcohol

2D ^{1}H – ^{13}C HSQC-NMR Two dimensional-heteronuclear single-quantum coherence-Nuclear magnetic resonance

XRD X-ray diffraction

Contents

1 Introduction

1.1 Importance of renewable energy

The possible future shortage of fossil-based resources, enhancement of greenhouse gases (GHG) emissions, and concerns regarding global climate change have boosted the interest towards a sustainable society. In order to reduce the GHG emissions in the EU, several goals have been set to reach net-zero emissions in 2050 as shown in Figure 1 [1]. According to official data reported in 2020, 32% lower GHG emissions were attained compared to 1990, which was a remarkable value below the target (20% reduction). However, it was followed by an upward trend in 2021, but still remained below pre-COVID-19 levels (2019). To achieve the milestone in 2030 with a continuous reduction up to 41%, implementation of the EU policy is pivotal.

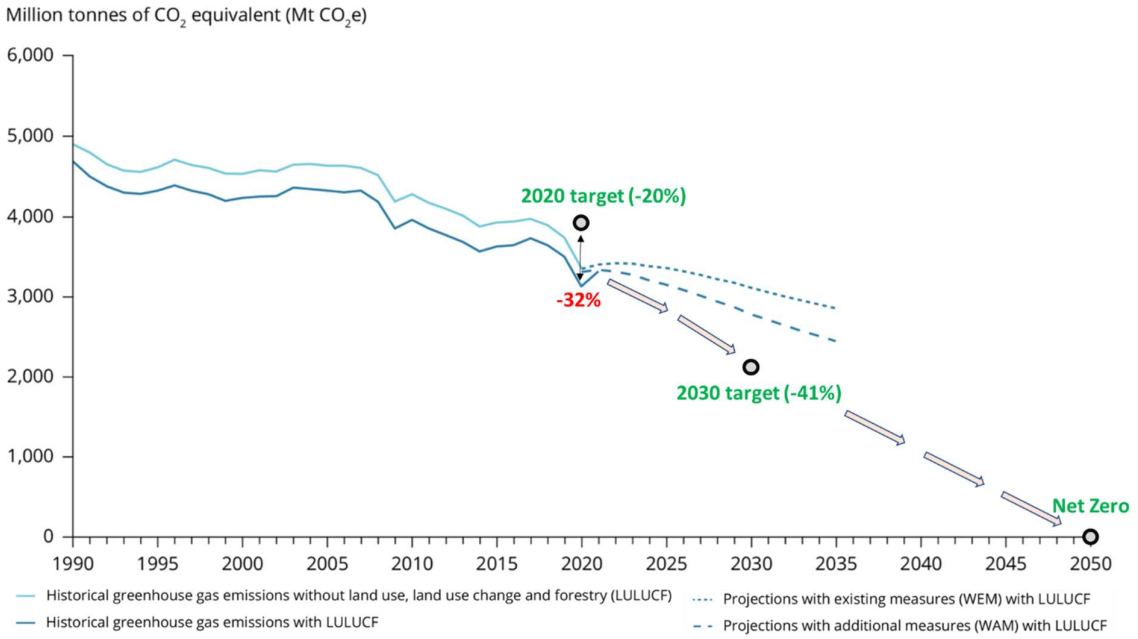

Figure 1. EU GHG emissions trend, and targets adapted from European Environment Agency [1]

Among various contributors, transport systems account for one of the main sectors where 25% of overall GHG emissions are owing to the burning of fossil fuels. This has led to increased interest in creating renewable/clean energy to achieve carbon neutrality. Wind, sun, solar, and biomass are energy sources that could be applied for this purpose. Liquid biofuels derived from renewable biomass are alternative sources to meet transportation fuel needs, particularly for heavy-duty vehicles and air transport. Their adoption has increased during the recent years, where the United States is producing the largest amount of biofuel in the world, succeeded by Brazil [2]. Furthermore, there are some biofuel producers mainly bioethanol and biodiesel in

Europe such as UPM-Kymmene Oyj, Green Fuel Nordic Oy, Preem AB, Neste, Svenska Cellulosa AB, Biomethanol Chemie Nederland BV, Beta Renewables SpA, Borregaard ASA, and others [3].

Generally, biofuels are categorized into four generations based on the type of biomass feedstock used and the production process as follows [4] (Figure 2):

The first-generation biofuels are derived from edible biomass such as starch, sugar, and vegetable oil. These are produced through upgrading processes, for instance fermentation, distillation, and transesterification. However, usage of such biomass competes with food crops, causing a threat to food prices, biodiversity loss, and water overconsumption. Accordingly, to overcome the drawbacks of the first-generation biofuels, second-generation biofuels using non-edible biomass from food waste, animal fat, and lignocellulosic biomass, as residues from agriculture and forestry were introduced [4]. The common upgrading processes for converting such feedstock include thermochemical processes such as pyrolysis, liquefaction, and gasification as well as biochemical conversion and hydroprocessing. Fast pyrolysis bio-oil processes are being prepared for commercialization for second-generation biofuels production [5]. The third-generation biofuels derived from algal biomass with high growth rates and oil productivity have attracted increasing attention. However, biofuel produced from algae is less stable in comparison to other sources due to its highly unsaturated algae-derived oil. The fourth-generation biofuels mainly use bioengineered microorganisms such as bioengineered algae or crops and are still in an early developmental stage.

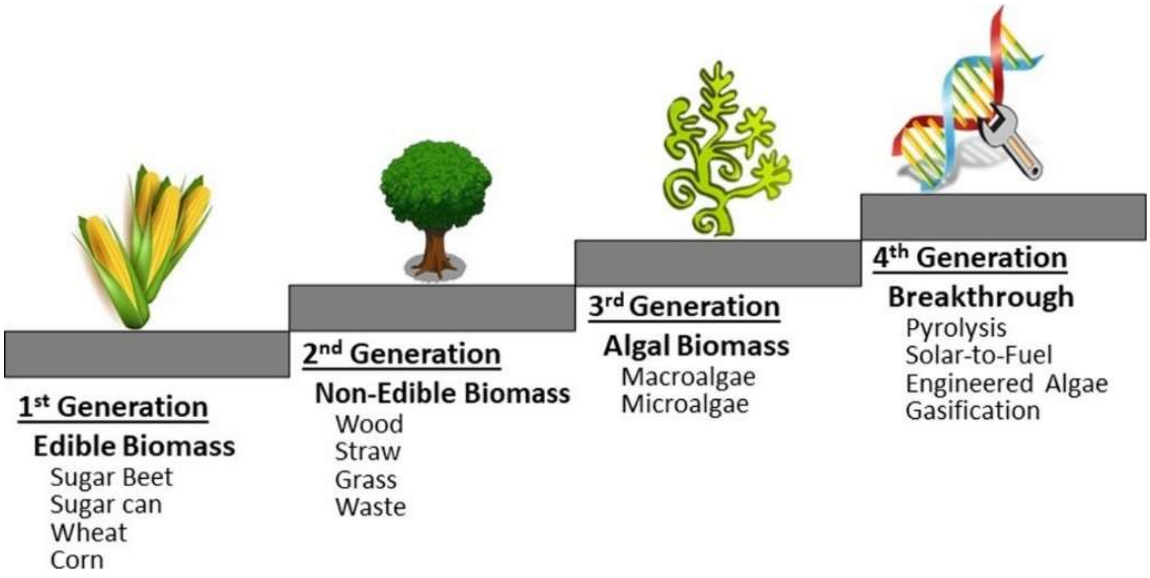

Figure 2. 1st, 2nd, 3rd, and 4th generation biofuels adapted from literature [4]

Currently, among various mentioned generations, first-generation liquid biofuels are considered the most cost-effective while the second-generation biofuels still have production cost limitations owing to high capital expenditure and low efficiencies of feedstock conversion to biofuel [6,7]. Therefore, further development in the production technologies of second-generation biofuels to enhance their cost-effectiveness is needed. In this study upgrading on second generation-biofuels through hydro processing is discussed.

1.2 Aim and scope

Pyrolysis oil derived from renewable lignocellulosic biomass is a complex mixture involving various organic oxygenated compounds, offering great potential for conversion to fuels/value-added chemicals. Solid/char formation is a major side reaction causing a lower yield of desired liquid products and the deactivation of the catalyst gradually during hydroprocessing. The aim of this work is to achieve a deep understanding of the stabilization of pyrolysis oil at mild conditions ($\leq 300°C$) and the parameters influencing carbon loss as solids. In the first study, a simulated pyrolysis oil was selected in order to examine the behavior of different oxygenates under mild thermal hydrotreatment, in the absence and presence of a catalyst (a conventional $NiMo/Al_2O_3$ catalyst). In the second study, the same feedstock was evaluated using various alumina supported catalysts (Pt, Pd, Rh, Re, and NiMo) under mild conditions in order to study their activity and selectivity for stabilizing reactive oxygenates.

1.3 Outline

Chapter 2 introduces the background of biomass-derived pyrolysis-oils, upgrading, and stabilization processes. It also includes a literature review on the stabilization of single model compounds and real and simulated pyrolysis oils.
Chapter 3 describes the details of the experimental protocol related to mild hydrotreatment along with characterization methods to analyze the products and catalyst materials.
Chapter 4 discusses the findings of both studies.
Chapter 5 and Chapter 6 present the conclusions and future outlook, respectively.

The summary of the scope of this research work is presented in Figure 3:

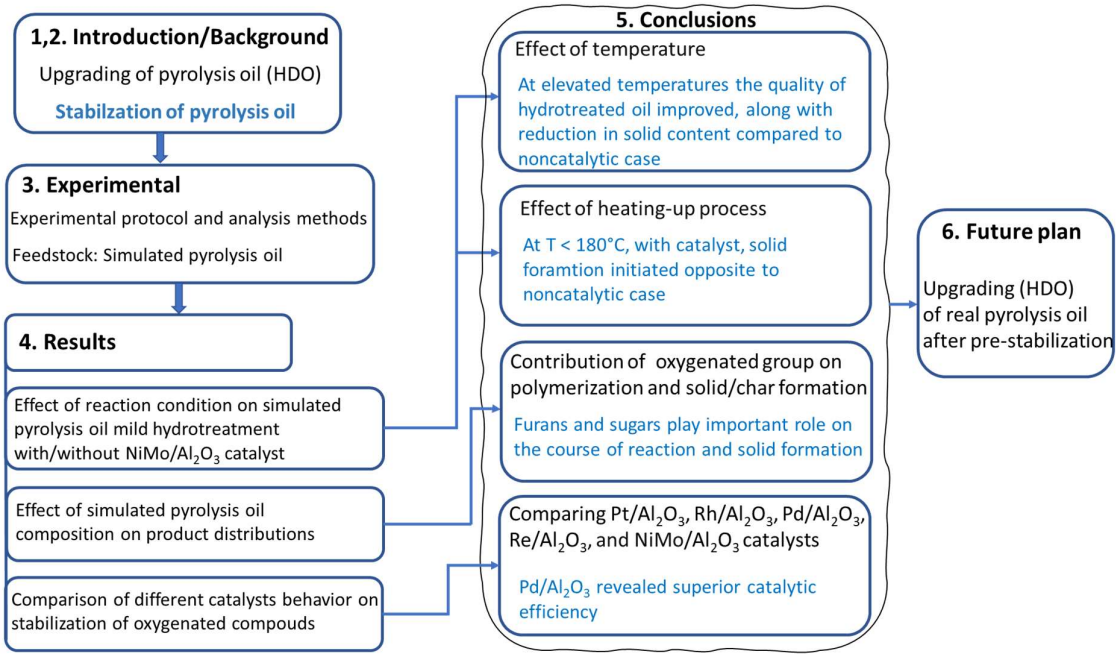

Figure 3. Recapitulation of this thesis as flowchart.

2 Background

2.1 Pyrolysis oil properties, upgrading, and stabilization

The utilization of renewable resources and the development of effective processes for their conversion into renewable fuels and bio-based chemicals has become of great interest in recent years. Lignocellulosic biomass (LCB) is a plant biomass, which is a highly renewable natural resource on Earth that has gained increased interest as a potential substitute to fossil feedstock. The valorization of such biomass entails the decomposition of its major components containing cellulose (40-50%), hemicellulose (25-40%), lignin (20-30%), and extractives through various technologies, depending on the choice of end-products. Fast pyrolysis is one of the most promising thermochemical processes to directly convert biomass to liquid in the absence of oxygen, at temperatures between 300-600°C, and a short residence time of less than 2 s with high yield of up to 75 wt%. Apart from bio-oil, the process produces bio-char, and volatile species. Bio-oil derived from fast pyrolysis is a dark red brown liquid, typically referred to as fast pyrolysis bio-oil (FPBO). It is a suitable source to produce biofuels due to its renewable and carbon-neutral features [8]. The chemical composition of pyrolysis oil largely depends on the biomass species, and pyrolysis process conditions (temperature, heating rate, and time). It is generally an extremely complex mixture that includes hundreds of organic compounds, including oxygen-containing organic groups (e.g., aldehydes, ketones, furans, sugars, acids, phenols, etc.) and up to 30 wt% water. This pool of oxygenates renders deteriorating properties such as:

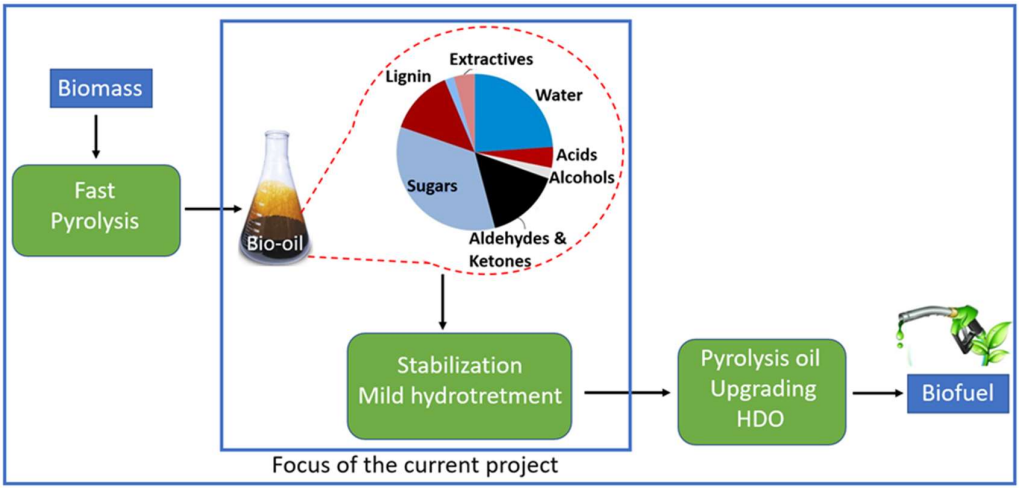

Figure 4. The stages of raw biomass transformation into a valuable product such as biofuel (pie diagram adapted from literature) [9]

high acidity, high viscosity, poor storage stability, low heating value and others. This makes pyrolysis oils undesirable for direct usage as transportation fuels and/or co-feeding with petroleum oils [10–12]. Therefore, pyrolysis oils need to be upgraded in order to yield deoxygenated products that are comparable with existing fuel grades. Pyrolysis oils can be upgraded via two main approaches: 1) catalytic cracking or 2) catalytic hydrodeoxygenation (HDO). The former requires the use of high temperatures (500-550°C) with acidic zeolite catalysts, resulting in high carbon loss as coke (> 20 wt%) and lowering the yield of the biofuel, which is not desirable [13]. Catalytic HDO is a promising method for this purpose. During this process, upgrading can be achieved via deoxygenation at elevated temperatures (> 300°C) with high hydrogen pressure and the presence of a selective hydrotreating catalyst. However, direct HDO under severe conditions cannot be directly adopted for pyrolysis oil, which is typically challenging due to the undesired condensation side reactions that also occur and are associated with high temperatures causing significant charring and deactivation of the catalyst.

To tackle this issue a two-stage HDO process using mild conditions (< 300°C) in the first step, prior to the severe hydrotreatment (300-400°C) in the second step, was developed and patented by Battelle for the HDO of bio-oil in 1989 [14]. The aim of the first stage, which is termed stabilization, is to stabilize pyrolysis oil via conversion of the most highly reactive compounds containing carbonyl and carboxyl functionalities, into more stable compounds, as quickly as possible before their reaction by condensation reactions forming high molecular weight compounds [10,15–18]. In the second hydrotreatment step the stabilized oils are subjected to more severe conditions using a conventional hydrotreating catalyst ($NiMo/Al_2O_3$ or $CoMo/Al_2O_3$) for cracking and HDO, and thus increasing the bio-oil quality. Using this approach, upgraded oils with very low oxygen contents (< 1 wt%) can be produced [9]. Subsequently, this two-stage hydrotreatment approach has been the focus of widespread research for upgrading oxygen-rich renewables to value-added products, along with suppressing char formation. The successive stages of biomass transformation into biofuel are simplified and shown in Figure 4, in which the stabilization step is the focus of the current project. The pyrolysis oil composition derived from pine wood was obtained from literature [9].

During the hydrotreatment of pyrolysis oil, a complex network of different reactions, which originate from the complicated composition of bio-oil, occurs. It involves two main reaction pathways in a parallel mode [19] as follows:

1) favorable hydrogenation, deoxygenation, decarboxylation, decarbonylation, hydrocracking, esterification, dehydration, hydrogenolysis, etc., which yield products with higher H/C and lower O/C ratios. These reactions depend heavily on a catalyst to occur at sufficient rates.

2) unfavorable crosslinking and non-catalytic polymerization reactions, due to reactive compounds that often occur with high rates without a catalyst, but can also be accelerated by a catalyst. This causes the formation of high molecular weight fragments and consequently char.

The rate of each path could be varied depending on the biomass derived-pyrolysis oil composition, the reaction conditions, and the catalyst applied. Figure 5 represents the general reaction network for catalytic hydrotreatment of pyrolysis oil.

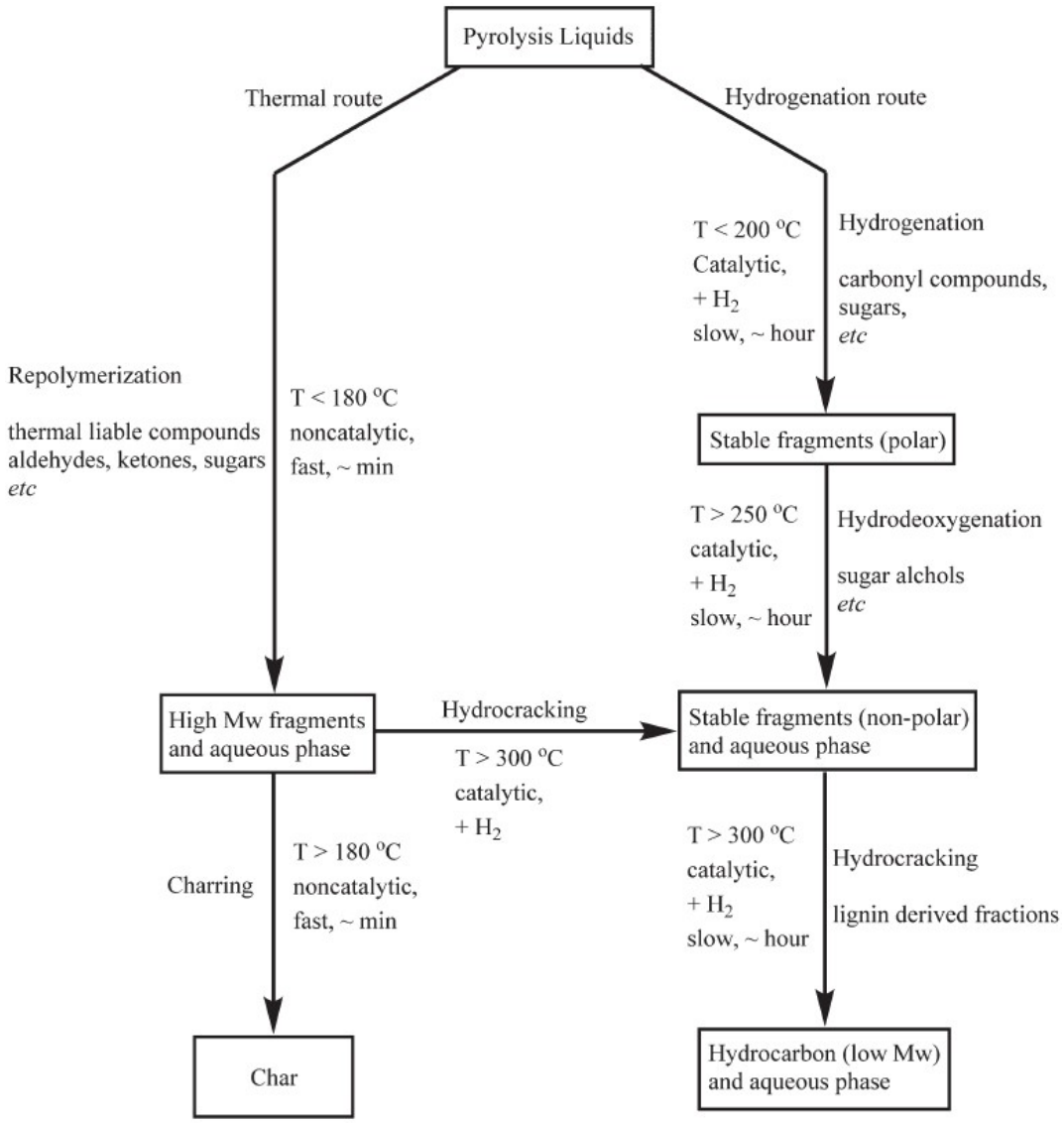

Figure 5. Proposed reaction pathway for the catalytic hydrotreatment of pyrolysis liquids adapted from literature [19]

There has been a great interest in studying the reaction network of the stabilization of pyrolysis oils over the past decades, which is essential for understanding the behavior of such oxygen-rich oils and particularly their tendency to char. However, due to a complex reaction network arising from the nature of pyrolysis oils, much research has been dedicated to studying single model compounds from various oxygenated groups present in pyrolysis oil, in lab-scale. The utilization of model compounds provides a quick estimate of the behavior of various oxygenated groups individually and the catalyst's performance on stabilizing them. However, there is a potential for cross-linking and cross-polymerization reactions occurring between oxygenated compounds in hydrotreatment of pyrolysis oil, which could promote the formation of large molecules leading to solids/char. Hence, the mixed model compounds intended to simulate pyrolysis oil, has been increasingly studied more recently to gain insight into how their composition affects selectivity, which helps to reveal the reaction mechanisms involved in real pyrolysis oil mild hydrotreatment.

In this thesis, in order to simulate pyrolysis oil more realistically a comprehensive mixture of hydroxyacetone, benzaldehyde, acetic acid, guaiacol, 5-hydroxymethylfurfural (HMF), and levoglucosan, were selected as representatives of ketones, aldehydes, acids, phenols, furans, and sugar compounds respectively in real pyrolysis oils. Their selection has been based on their abundance in the corresponding oxygenated groups found in the literature [20–23]. The thermal-non catalytic and catalytic hydrotreatment of the simulated pyrolysis oil mixture in the absence and presence of the catalyst was studied at mild conditions (180-300°C).

2.2 Mild hydrotreatment/Stabilization of pyrolysis oils and their model compounds

The progression of various reactions during mild hydrotreatment depends strongly on the type of catalyst used and operating conditions (heating process, temperature, pressure, reaction time, and solvent). Pyrolysis oil molecules and hydrogen are initially adsorbed on the metal active sites of the fresh catalyst, which is followed by the hydrotreatment reactions, along with cracking whereas various polymerization reactions can also occur without the catalyst. Through these reactions, hydrotreated products and the precursors of char-like material are formed simultaneously in the hydrotreatment. Char formation ends up blocking the active sites and plugging the catalyst pores, which reduces the activity of the catalyst gradually. The most commonly tested catalysts for stabilization of pyrolysis oil and model compounds are noble metal catalysts, due to their high hydrogenation efficiency to eliminate the highly reactive

compounds under mild conditions [9,10]. However, transition metal sulfide catalysts, typically molybdenum supported on alumina and promoted by nickel or cobalt ($NiMo/Al_2O_3$ or $CoMo/Al_2O_3$), are conventional hydrotreatment catalysts employed for HDO, however, they still could be sufficiently active at lower temperatures [9]. Various noble metals (Pd, Pt, Ru, Rh, etc.) over different supports such as metal oxides (TiO_2, Al_2O_3, SiO_2, Fe_2O_3, ZrO_2), and particularly activated carbon have been used at milder conditions [9,10,24–31]. Activated carbon offers advantages including its large surface area and high porosity, but its disadvantage is that it is difficult to regenerate due to its lower stability under extreme or oxidizing conditions that are usually needed for char removal. There are many studies related to the use of alumina as a relatively inexpensive support with good textural and mechanical properties [32,33]. Its acidic properties are also known to be effective for breaking the C-O bonds in pyrolysis oil compounds during catalytic hydroprocessing. This section presents a brief review of studies on mild hydrotreatment of pyrolysis oils and their model compounds over alumina-supported catalysts in the temperature ranges of 150-300°C.

Kadarwati *et. al* studied [34] the stabilization of mallee wood derived-pyrolysis oil using a sulfided $NiMo/Al_2O_3$ catalyst at low temperatures (150-300°C) and its effect on undesired char/solids. It was found that compared to the catalyst-free experiment, the catalyst could diminish the solid formation and oxygen content by ca. 56% in the stabilized oil at 300°C [34]. However, their study did not report detailed information about the nature of the solid product and the effect of the pyrolysis oil composition on solid/char formation. In another study, the effect of a noble metal on stabilization of bio-oil obtained from pyrolysis of Leucaena leucocephala was assessed at mild conditions (300°C, 2 bar N_2, 1h) [35]. They concluded that the Pt/Al_2O_3-catalytic deoxygenation successfully reduced the oxygen content in stabilized oil from a molar O/C ratio of 0.43 to 0.18 via C-O bond cleavage to form hydrocarbons and water after deoxygenation. Also, compared to elevated temperatures, the degree of repolymerization of oxygenates in pyrolysis oil decreased and a solid yield of 28 wt% was obtained [35]. Furthermore, the promising results were demonstrated in another study [24] using a traditional $NiMo/Al_2O_3$ catalyst on the stabilization of pyrolysis oil derived from beech wood at 250°C, 100 bar hydrogen over 4 h reaction. The $NiMo/Al_2O_3$ catalyst was superior compared to Ru/Al_2O_3 and resulted in a higher yield of stabilized oil, 31 wt% compared to 24 wt% using Ru, and a deoxygenation level with 0.31 O/C molar ratio in the presence of $NiMo/Al_2O_3$ compared to 0.38 for Ru/Al_2O_3 [24].

Various catalytic systems have been reported for determining the conversion and selectivity of oxygenated model compounds present in pyrolysis oil. In the literature, guaiacol has been widely chosen as a lignin monomer to study its behaviour during mild hydrotreatment using different noble metal catalysts [36,37]. Lee *et al.* [36] concluded that among SiO_2-Al_2O_3 supported Pd, Rh, Ru, and Pt, guaiacol was completely converted in the presence of Rh and Ru, with the highest selectivity being towards hydrogenation of aromatic rings, followed by the deoxygenation process to yield cyclohexane at 250°C. In another study by He *et al.* [37] on guaiacol mild hydrotreatment at 285°C, 4 MPa hydrogen, and 4 h reaction, $NiMo/Al_2O_3$ showed a better performance than a noble metal (Pt/Al_2O_3) with higher activity and selectivity towards a deoxygenated product, cyclohexane (67 compared to 42 wt%) along with diminishing coke formation. Hydrodeoxygenation reportedly occurred due to a synergy effect of the metal sites on hydrogen molecule dissociation and acid sites of Al_2O_3 for dehydration of cyclohexanol to cyclohexene [37]. Zanuttini *et al.* [38] also highlighted Pt/Al_2O_3 as an effective catalyst for cresol deoxygenation. They reported that Pt loading plays an important role on the product distribution during hydrotreatment at 300°C and atmospheric pressure with lower coke yield at high contents of Pt. The desired deoxygenated product, toluene, was produced via dehydroxylation of m-cresol either by dehydration on the acid sites or by HDO on the Pt sites [38]. In another study done on catalytic hydrotreatment of a cyclic ketone, cyclohexanone at 300°C using Pt/Al_2O_3, phenol was reported as the dominant product via dehydrogenation with a selectivity up to 90%. It was however, accompanied by condensation reactions that resulted in a minimal yield of coke (< 0.08 %) [39]. Bhogeswararao *et al.* [40] compared Pt and Pd over Al_2O_3 in hydrotreatment of furfural at 240°C and 20-60 bar hydrogen. Pd/Al_2O_3 revealed decarbonylation of furfural giving furan in 82% yield, whereas Pt/Al_2O_3 facilitated hydrogenolysis of C=O and C-O groups to yield 2-methylfuran (2-MF) that coincided with products of furan ring-opening [40]. A catalyst screening was performed [41] on a pool of non-furanic carbonyl groups, comprising acetaldehyde, propanal, acetone, xylose, and furanic compounds such as furfuryl alcohol, tetrahydrofurfuryl alcohol (THFA) in the presence of various noble metal catalysts (alumina-supported Ru, Pd, Pt, and Rh) and Ni/Al_2O_3. Ru/Al_2O_3 (3 wt%) appeared as a superior catalyst for the hydrogenation of non-furanic carbonyl groups. However, polymerization was the dominant reaction during the catalytic hydrotreatment of a furan such as THFA using Ru which led to sever coking. Oppositely, the Pd was the most active metal for hydrogenation of carbonyl groups attached to furan rings. The Pd/Al_2O_3 catalyst showed to have the highest initial rates in the hydrotreatment of furanic carbonyl groups in furfural (0.128 s^{-1}) and the C=C bonds in furfuryl alcohol (0.076 s^{-1}). The reduction in the initial activity for hydrotreatment of furfural

was reported to be as follows: Pd∼Ni > Ru > Pt > Rh [41]. During thermal hydrotreatment of pyrolysis oil on the other hand, carboxylic acids were found to behave as acid catalysts for promoting polymerization. Comparing various carboxylic acids, acetic acid, due to its weak acidity had an insignificant influence on enhancing polymerization [42–44].

2.3 Mild hydrotreatment/Stabilization of simulated pyrolysis oil

During recent years, some studies have been dedicated to the mild hydrotreatment of mixed model compounds as simulated pyrolysis oil, however, all oxygenated groups have not been taken into consideration [16,45,46]. To be specific, mixtures of acids and phenols were assessed in one study [45] while representatives of acids, furans, phenols, and ketones in a mixture was another case study [16]. Furthermore, representatives from ketones, furans, and phenols were mixed and placed as a different case study [46]. A mixture of acetic acid and p-cresol was employed by Wan *et al.* [45] to mimic pyrolysis oil using Ru/C at 300°C and 48 bar H_2. According to their observations, p-cresol HDO was favoured in the presence of acetic acid, while hydrogenation of acetic acid was suppressed with p-cresol [45]. In another study [16], stabilization of a simulated pyrolysis oil comprising furfural, guaiacol, acetic acid, phenol, and hydroxyacetone was evaluated over Pt-Fe, Pt-Ni, Pd-Fe, and Pd-Ni catalysts supported on SiO_2 at 240-300°C, using ethanol as an H-donor solvent. Pt-Fe/SiO_2 and Pt-Ni/SiO_2 were highlighted as high-performance catalysts in terms of the conversion of acid-rich pyrolysis oil and the hydrogenation of pyrolysis oil rich in phenols, respectively [16]. Analysis on liquid products indicated the occurrence of various reactions as depicted via a proposed reaction scheme over bimetallic catalysts. Hydrogenation of the carbonyl group in furfural was seen using all catalysts, although it was followed by isomerization to yield 3-methyl-furan using Pt-Fe, and Pd-Fe and the furan ring hydrogenation over Pt-Ni, and Pd-Ni due to the strong interaction between the furan ring and Ni, and Pd. The coke yield ranged from 1.1 to 1.9 wt%, however, no information was reported regarding its composition [16]. The interactions between oxygenates in the mild hydrotreatment of a simulated pyrolysis oil involving phenol, furfural, and hydroxyacetone were studied [46] over Ni/SiO_2, at 180°C and 3.5 Mpa H_2. The conversion of hydroxyacetone and particularly phenol was inhibited by furfural due to its strong adsorption on the surface of the Ni/SiO_2 catalyst [46].

The non-catalytic-thermal reactions between oxygenates in pyrolysis oil were also assessed during thermal treatment [42,43,47,48]. Xu *et. al* reported [21] the increment in the cross-polymerization between furfural and phenolics during thermal treatment at 200°C, and 30 bar

N_2, due to the presence of stronger acids, such as H_2SO_4 and benzoic acid. The occurrence of such undesirable reactions between furans and phenolics was also found by Sun *et. al* [47] even during a transient heating process taking 0.5 h up to 200°C with higher reactivity of furans towards polymerization. Apart from phenols, the cross-polymerization between furans and carbohydrates was also confirmed during thermal treatment at 200°C and 40 bar N_2, in which the polymer obtained from sugars was more aliphatic than that from furans. Also, the presence of acetic acid caused an increase in the formation of heavier insoluble polymers [43]. In another work different oxygenates such as HMF, furfural, vanillin, guaiacol, xylose, methanol, hydroxyl acetone, furan, and furfuryl alcohol were evaluated by their addition to a pyrolysis oil individually during thermal treatment at 170-280°C [48]. Among all tested oxygenates from different organic groups, HMF and furfural were found to be the most effective polymerization agents that significantly enhanced the solid yield [48]. These last studies present a simplified modeling of pyrolysis oils for analysis of their behavior, vital for further understanding of pyrolysis oils stabilization. However, all oxygenated groups were not included in the feedstock mixtures, and more importantly their role in influencing the nature of products and their qualities during the stabilization step is still ambiguous.

This thesis deals with understanding the behavior of major oxygenated groups with various functionalities present in pyrolysis oil during thermal and catalytic mild hydrotreatment using various catalysts. This helps to draw the whole picture for understanding the reaction behaviors of real pyrolysis oil especially unfavorable carbon loss as solids.

3 Experimental

This chapter presents the catalysts synthesis method, materials applied in both papers, experimental protocol, and characterizations methods including BET, XRD, ICP-SFMS, and NH_3-TPD for catalysts, GC-MS, Karl Fisher titration, MALDI-TOF MS, 2D-HSQC-NMR, and elemental analysis used for products.

3.1 Catalysts synthesis

Monometallic and bimetallic ɤ-alumina supported catalysts comprising Rhodium (Rh), Rhenium (Re), Palladium (Pd), Platinum (Pt), and Nickel-Molybdenum (NiMo) were synthesized using a conventional incipient wetness co-impregnation method. The ɤ-alumina (Puralox SCCA 150/200, Sasol), with a surface area of 192.3 m^2/g was calcined at 550°C for 8 h. An aqueous solution containing metal precursors, ammonium perrhenate (NH_4ReO_4), rhodium (III) nitrate solution ($Rh(NO_3)_3$, platinum (IV) nitrate solution, and tetra ammine palladium (II) nitrate $N_4O_{12}Pt$, and Ni $(NO_3)_2.6H_2O$ and $(NH_4)_6Mo_7O_{24}.4H_2O$ (Sigma-Aldrich) were prepared. 5 and 15 wt % loadings of Ni and Mo for bimetallic catalysts and 2 wt% loading for monometallic catalysts were added dropwise to pre-calcined alumina support. In addition, in **paper II**, for another Pd catalyst with 5 wt% metal loading similar steps were followed. Afterward, the catalysts were dried first at 60°C overnight for 12 h and then at 110°C for 12 hr, with subsequent calcination at 550°C for 12h with a heating rate of 2°C/min. Prior to the reaction, the calcined NiMo/ɤ-alumina catalyst was sulfided with dimethyl disulfide (DMDS, ≥ 99%, Sigma-Aldrich) at 340°C and 20 bar hydrogen for 4 h in a Parr autoclave reactor to be activated. However, all calcined noble metals and Re catalysts were reduced at 300°C and 15 bar hydrogen for 4 h followed by passivation in a 2% O_2/N_2 flow (25 ml min^{-1}) for 1 h. The resulting sulfided ɤ-alumina-supported NiMo and reduced Rh, Re, Pd, and Pt catalysts were marked as NiMo, Rh, Re, Pd, and Pt catalysts.

3.2 Materials (Feedstock, solvents, catalysts)

The abundant oxygen-containing organic compounds present in pyrolysis oil are classified into some main groups including sugars, acids, furans, aldehydes, ketones, and phenols. The complex mixture of pyrolysis oil was simulated by using a representative from each main oxygenated compound group, in a mixture comprising the different functional groups. Levoglucosan (Carbosynth), acetic acid (≥99.7%, Sigma-Aldrich), HMF (Sigma-Aldrich), benzaldehyde (≥ 99%, Sigma-Aldrich), hydroxyacetone (95%, Sigma-Aldrich), and Guaiacol

(≥98%, Sigma-Aldrich), were the model compounds for sugars, acids, furans, aldehydes, ketones, and phenols, respectively. The six compounds were mixed in equal masses to make the feedstock (6 g total) for hydrotreatment experiments, and the mixture is referred to as the simulated pyrolysis oil as shown below in Figure 3. Hexadecane was used as an inert solvent (150 ml, 99%, Sigma-Aldrich). In **paper I,** the $NiMo/Al_2O_3$ catalyst was employed along with dimethyl disulfide (DMDS, grade ≥ 99%, Sigma-Aldrich) as a sulfiding agent. In **paper II** various catalysts (Pd/Al_2O_3, Pt/Al_2O_3, Rh/Al_2O_3, Re/Al_2O_3) were also evaluated.

3.3 Mild hydrotreatment experimental protocol

The mild thermal and catalytic hydrotreatment experiments were carried out in a batch reactor (450 ml, Parr instrument) equipped with a magnetically driven internal stirrer. For catalytic experiments, 1 g catalyst and 150 ml of Hexadecane solution containing the mixture of the above-mentioned six model compounds (each 1 g), were introduced into the reactor along with the sulfidation treatment via adding DMDS for the NiMo catalyst and reduction and passivation for the noble metal and Re catalysts. To explore the effect of the catalyst on the stabilization process, blank experiments with identical reaction conditions were also conducted. After loading the feedstock, the reactor was initially pressurized/depressurized with N_2 three times to remove air followed by flushing with H_2 at 15 bar repeated three times, and ultimately the reactor was charged with 30 bar of H_2 at room temperature. In the first part of **paper I**, the effect of temperature on mild hydrotreatment using the NiMo catalyst was evaluated. Accordingly, different reaction temperatures under mild conditions such as 180, 210, 250, and 300°C were tested at a stirring rate of 1000 rpm. After reaching the setpoint temperatures, the pressure was adjusted to 60 bar for all experiments to keep the same pressure while continuously stirring. After the pre-set reaction time (4 h), the reactor was rapidly cooled down to room temperature with a water bath and then depressurized. In the second part of **paper I**, for analyzing the effect of the heating-up process, the reaction was stopped immediately after reaching the setpoint of 180°C after an average heating rate of 12°C/min. Upon reaching 180°C, rapid cooling of the reactor was started, by cooling water flowing through an internal coil, to stop reactions. In **paper I** the study continued by a set of experiments with/without NiMo catalyst, at 180°C, 60 bar H_2 and 4 h reaction where reactants were removed one by one, but with the total mass of feedstock always constant. In these experiments, to be able to compare the results with the experiment with all 6 reactants, the mass of each reactant was 1.2 gr. In **paper II**, a catalyst screening study was done on the stabilization of the same simulated pyrolysis oil mixture with similar quantity. The vessel containing products was weighed and

compared with the weight of the vessel with feed solution inside and the empty vessel. The residue yield obtained from their difference was about 1.3-1.8 wt%, indicating any loss due to vaporization or gas product formation was very low. Two immiscible liquid products containing a yellowish organic phase rich in hexadecane, a dense browny phase, and a sticky solid product were obtained. These fractions were extracted and analyzed according to the experimental protocol illustrated in Figure 6 in both **papers I** and **II**. The solid product along with the catalyst were recovered after filtration and washed with acetone. It was then dried, weighed, and labeled as 'total solid product' after subtracting 1 g, to account for the catalyst. At the same time, the dense browny phase was separated from the yellowish organic liquid fraction and then was added to the acetone fraction, weighed, and referred to as the aqueous phase. The water in the aqueous and organic phases was measured by volumetric Karl-Fisher titration. The acetone was removed from the aqueous phase and the remaining dense organic mixture was diluted by isopropanol. Ultimately, hexadecane and isopropanol solutions were mixed with a 1:1 v/v ratio to make a uniform solution for GC-MS analysis. Furthermore, the collected total solid product was further analyzed by using two consecutive steps, that first involved extracting the solid products into soluble and insoluble (char) fractions via dimethyl sulfoxide (≥99.9%, VWR, DMSO) as an extraction solvent. The dark-colored soluble solid was collected and subjected to 2D-HSQC-NMR and MALDI for further analysis. The final solid residue after rinsing with acetone, and drying, was weighed and considered as the insoluble solid (char) after subtracting the original catalyst mass (1 g). Elemental analysis was carried out for measuring its composition.

3.4 Liquid and solid products analysis

3.4.1 Gas Chromatography-mass spectroscopy (GC-MS)

The liquid phase products from catalytic and thermal mild hydrotreatment were analyzed using a one-dimensional gas chromatography-mass spectroscopy system (GC-MS, 7890- 5977A, Agilent) and detected by a mass spectrometer (MSD) detector. The GC-MS had a mid-polar VF-1701MS column (30 m × 250 μm × 0.25 μm) and a non-polar DB-5MS column (1.2 m × 150 μm × 0.15 μm). Mass Hunter data with the NIST library was used to identify the compounds from the analysis. The initial oven temperature was kept at 40°C for 2 min and then increased to 100 °C with a rate of 3°C/min and was maintained for 3 min. Then it was heated to 170°C with a rate of 3 °C/min and was ramped to 270°C with a rate of 10°C/min continuously. A six-point calibration was carried out with pure components, giving calibration

curves with R^2 values above 0.99 to quantify the compounds in the feedstock and reaction products.

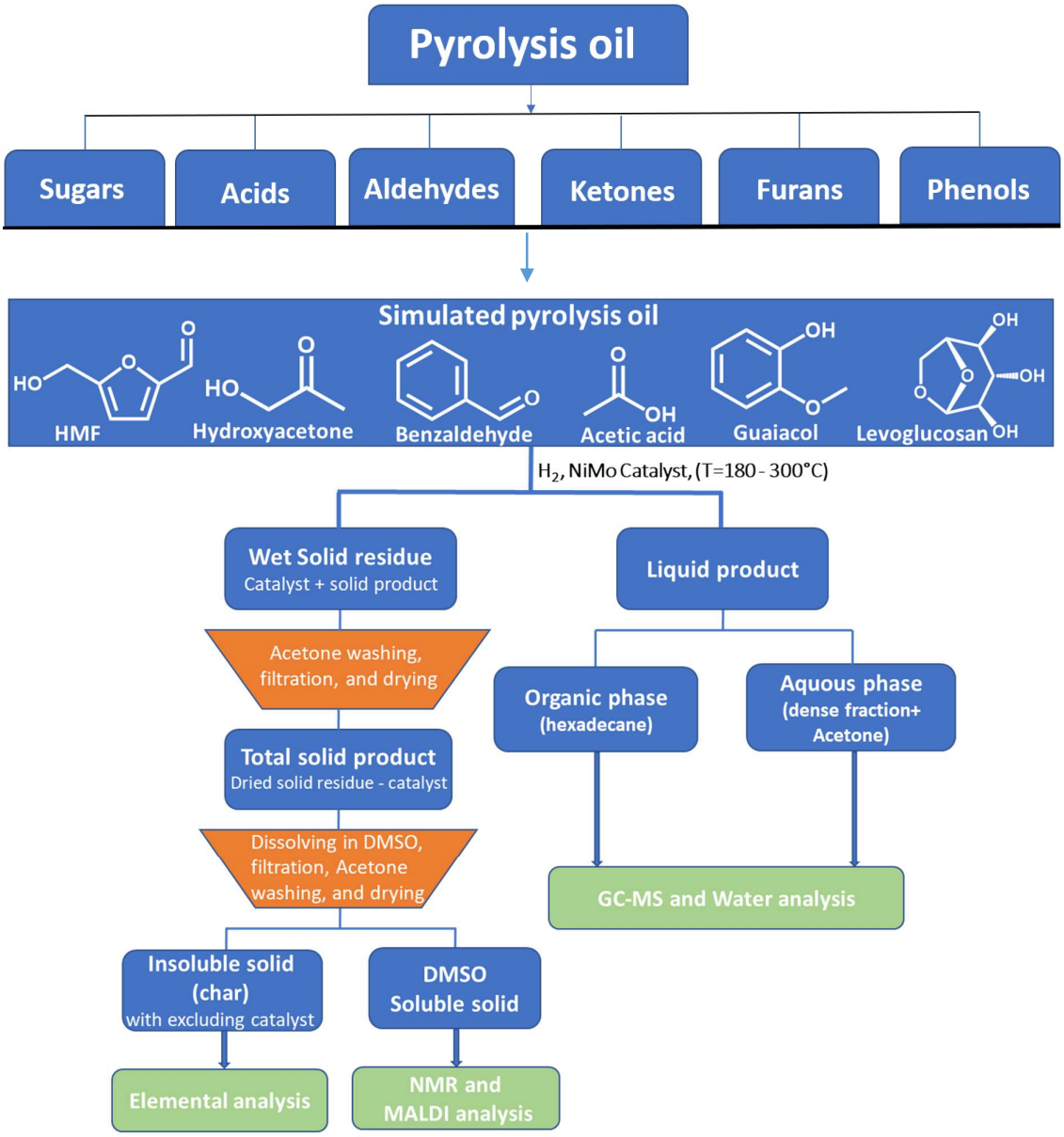

Figure 6. Scheme of the steps followed for collecting products and their characterization

Conversion and yield of reactants and products were calculated according to the following equations:

$$\text{Conversion of oxygenates}\ (\%) = \left(1 - \frac{\text{Mass of oxygenates in product}}{\text{Mass of oxygenates in feed}}\right) \times 100\ \% \quad (1)$$

$$\text{Yield } \textit{GC/MS detectable liquid product}\ (\%) = \frac{\text{Mass of light products detected by GC/MS}}{\text{Mass of simulated pyrolysis oil feed}} \times 100\ \% \quad (2)$$

$$\text{Yield } \textit{Solid product (\%)} = \frac{\text{Mass of solid product}}{\text{Mass of simulated pyrolysis oil feed}} \times 100\ \% \quad (3)$$

$$\text{Yield } \textit{Insoluble solid (\%)} = \frac{\text{Mass of insoluble solid}}{\text{Mass of simulated pyrolysis oil feed}} \times 100\ \% \quad (4)$$

$$\text{Yield } \textit{Water (\%)} = \frac{\text{Mass of water}}{\text{Mass of simulated pyrolysis oil feed}} \times 100\ \% \quad (5)$$

$$\text{Yield } \textit{unreacted simulated pyrolysis oil (\%)} = \frac{\text{Mass of remain reactants detected by GC/MS}}{\text{Mass of simulated pyrolysis oil feed}} \times 100\ \% \quad (6)$$

Also, the yield of high molecular weight soluble oligomers in the liquid product (GC/MS undetectable compounds) were calculated as follows:

$$\text{Yield } \textit{liquid oligomeric products (\%)} = 100 - \text{Yield } \textit{GC/MS detectable liquid product} - \text{Yield } \textit{solid product} - \text{Yield } \textit{water} \quad (7)$$

3.4.2 Volumetric Karl-Fischer titration

Water content of the hydrotreated oils was determined using a Metrohm 870 KF volumetric Karl-Fischer titrator V20. The sample (≈0.1-0.2 mg) was titrated with Karl Fischer titrant (HYDRANAL™ - Composite 5, Honeywell Fluka™). All measurements were performed in triplicates and average values were reported.

3.4.3 2D-HSQC- NMR

Two dimensional (2D) $^{1}H–^{13}C$ heteronuclear single-quantum coherence nuclear magnetic resonance spectroscopy, (HSQC)-NMR, is used in **paper I** to determine the structure of the soluble solids. The samples were initially dissolved in deuterated dimethyl sulfoxide (DMSO-d_6) with the ratio of 9:1 (v/v) for chemical shift calibration and transferred to NMR tubes to be analyzed. Spectra were recorded at 25°C using an 800 MHz spectrometer equipped with a 5 mm TXO cold probe (Bruker Avance III HD; Bruker BioSpin GmBH, Rheinstetten, Germany). 2D ^{1}H – ^{13}C HSQC spectra with suppression of the DMSO signals were used with 96 ms acquisition time for ^{1}H and 8.4 ms for ^{13}C and an interscan delay D1 of 2.5 s, where 4 or 8 scans were run depending on the sample concentration. The NMR spectra plotting were accomplished using standard Bruker Topspin-NMR software. A similar analysis was included for the soluble solids and stabilized oils obtained from experiments in **paper II**.

3.4.4 MALDI-TOF MS

The Matrix Assisted Laser Desorption Ionization Time of Flight Mass Spectroscopy (MALDI-TOF MS) technique was used due to its rapid and accurate identification of large molecules in liquids or dry solids giving the molecular weight (M_w) distributions of the compounds, which

allows the possible ranges of structures of large molecules to be understood. Before the analysis, the sample must be diluted by a matrix to protect the sample from direct laser irradiation. MALDI-TOF was conducted in a Bruker Autoflex Ultraflextreme MALDI in a positive mode, with 2,5-dihydroxybenzoic acid (DHB) as the matrix.

The DMSO soluble solids collected from extracting solid products in **paper I** were evaluated by MALDI-TOF spectroscopy within the molecular weight range of 200 to 4000 m/z. The samples were prepared as follows: i) 0.04 g of soluble solid was dissolved in 1000 µl of a 4:1 v/v acetone/water solution. ii) A matrix solution was prepared by adding 0.01 g of the matrix (DHB) to 1000 µl Acetone. iii) The first prepared solution was mixed with the matrix solution in a 1:1 v/v ratio. vi) 1 µl of the resulting mix was placed on the MALDI plate and left overnight at room temperature for solvent evaporation. The MALDI plate containing the dry droplet samples was introduced into the spectrometer for analysis/measurement. Reproducibility was determined, and the average value was reported.

3.4.5 Elemental analysis

A Vario micro-cube Elementar instrument analyzer was employed in **paper I** to determine the compositions of carbon (C) and hydrogen (H) of the insoluble solids (char) containing the catalyst. The samples were combusted at 1150°C using oxygen during the analysis. The gaseous combustion products were blown by Helium as a carrier gas to be quantified with TCD detectors. The molar C/H ratio was calculated to predict the insoluble solid/char structure. A similar evaluation was also carried out for corresponding samples in **paper II**.

3.5 Catalyst Characterization

3.5.1 Inductively coupled plasma and Mass spectroscopy (ICP-SFMS) analysis

For quantification of the metal contents NiMo, Pd, Pt, Rh, and Re on the Al_2O_3 support, the Inductively Coupled Plasma-Sector Field Mass Spectroscopy (ICP-SFMS) technique was used, as carried out by ALS Scandinavia AB, Luleå, Sweden.

3.5.2 X-ray diffraction (XRD)

The crystallinity of the synthesized catalysts was characterized by X-ray diffraction (XRD) spectrometry in this study. X-ray diffractograms were obtained using a Bruker AXSD8 Advance diffractometer operated at 40 kV and 40 mA with a CuKα monochromatic radiation (λ = 1.542 Å) and in the two-theta range of 5 to 90 degrees with a scan mode of 0.03°.

3.5.3 Brunauer-Emmett-Teller (BET)

The textural properties of synthesized catalysts in **papers I** and **II** (including specific surface area, pore volume, and mesopore sizes) were determined via the BET (Brunauer–Emmett–Teller) and BJH (Barrett-Joyner-Halenda) methods. Before the measurement, the catalysts were degassed under nitrogen flow overnight at 250°C.

3.5.4 Temperature-programmed desorption (TPD) of ammonia (NH_3)

NH_3-TPD was carried out to measure the total acidity and distribution of acidic site strengths of the NiMo catalyst in **paper I.** The NH_3-TPD system consisted of mass flow controllers (MFC), a quartz tube containing the catalyst sample in a temperature-controlled oven, and a mass spectrometer (MS) to monitor the NH_3 content of the outlet gas. For NH_3 adsorption, 30 mg of catalyst was loaded into the quartz tube and was treated with Argon gas, followed by exposure to a gas stream containing NH_3 at 100°C for 2 h. Thereafter to remove excess physisorbed NH_3, the catalyst sample was flushed under a flow of pure Argon at the same temperature for 1 h, followed by desorption with a temperature ramp of 10°C min^{-1} to 800°C. The amount of desorbed NH_3 under the Argon flow was measured with a mass spectrometer (MS, Hiden HR20). Acid site strength distribution was determined by calculating the quantity of desorbed NH_3 in different temperature ranges: weak, < 250°C; medium, 250-350°C; strong, > 350°C.

4 Results and Discussion

This chapter is allocated to evaluating the results obtained from two studies presented in **Papers I** and **II**. In **Paper I** the performance of a $NiMo/Al_2O_3$ catalyst was studied for stabilization of simulated pyrolysis oil and compared to catalyst-free experiments under mild conditions. The effect of three parameters on simulated pyrolysis oil conversion was scrutinized. In the first study of **paper I**, the effect of temperatures (180, 210, 250, 300°C) on simulated pyrolysis oil hydrotreatment was examined at 60 bar H_2 pressure and 1000 rpm stirring rate for 4 h with/without NiMo catalyst. The effect of the heating-up process to reach the desired set point temperature of 180°C with/without NiMo catalyst was the second examined parameter. The third study of **paper I** was the determination of the effect of simulated pyrolysis oil composition on product distributions. The characterization tests applied for catalysts and products are demonstrated and discussed here. For all experiments in **papers I** and **II**, simulated pyrolysis oil conversion, and different products yields were calculated. The liquid products obtained from all experiments are composed of GC detectable and undetectable compounds corresponding to light compounds and heavy oligomers produced during hydrotreatment. For simplicity, hydrocarbons, and oxygenated compounds detected by GC/MS in the liquid products were classified into various groups, namely oxygen-free, ketones, acids, phenols, alcohol, furan (furan-ring compounds), ester, ether and multiple oxygen groups compounds that contained more than one oxygenated functional group. A scheme for the reaction network of series and parallel reaction pathways taking place during mild hydrotreatment of simulated pyrolysis oil over sulfided NiMo catalyst will be proposed.

The same experimental protocol has been used for **paper II**. This study focuses on the behavior of different types of noble metal catalysts (Rh/Al_2O_3, Pd/Al_2O_3, and Pt/Al_2O_3) compared to Re/Al_2O_3 and conventional sulfided $NiMo/Al_2O_3$ catalysts during mild hydrotreatment of simulated pyrolysis oil at 180°C, 60 bar H_2 pressure, and 4 h reaction. Moreover, how the properties of the catalysts can influence the interactions between different compounds present in simulated pyrolysis oil was investigated. Also, a comparison was made between blank and catalytic experiments using different catalysts.

4.1 Stabilization of simulated pyrolysis oil under mild conditions over $NiMo/Al_2O_3$ catalyst

4.1.1 Effects of reaction temperature on products distribution and characteristics

4.1.1.1 Conversions and product distribution yields

Figure 7 shows the pyrolysis oil conversion, and yield of products including water, solid, and hydrotreated oil (liquid product) obtained at different temperatures of 180, 210, 250, and 300°C using the NiMo catalyst, after 4 h reaction. Almost 100% conversion of HMF, Hydroxyacetone, and levoglucosan was obtained at all temperatures, whereas other oxygenates such as benzaldehyde and guaiacol showed low conversion below 20%, along with 70 % conversion of acetic acid at 180°C. At elevated temperatures, benzaldehyde's conversion remarkably improved and reached 100% conversion at 250°C while acetic acid showed a slightly increasing trend. Guaiacol in the simulated pyrolysis oil mixture indicated the lowest conversion at mild conditions, 17.3% at 180°C to 31% at 300°C which is in line with previous literature [34]. The yields of liquid product (composed of GC detectable compounds and heavy oligomers) and water were enhanced while solid yield was reduced at higher temperatures. Even though, water content is slightly decreased when the temperature rose from 180 to 210°C, which might be ascribed to the higher rate of hydrolysis reactions at 210°C [49]. As depicted in Figure 4, the yield of GC detectable compounds progressed from 19.9 wt% at 180°C to 46.3 wt% at 300°C and the lowest fraction of heavy oligomers (1.2 wt%) was obtained at higher temperatures i.e., 300°C. These results imply that in the presence of the NiMo catalyst hydrogenation and cracking reaction rates are increasing at elevated temperatures due to decomposition of solid precursors. Unlike higher temperatures, at lower temperatures of 180 and 210°C, the rate of condensation and subsequent oligomerization reactions sounds higher leading to the formation of higher yields of oligomers and solid products, particularly at 180°C.

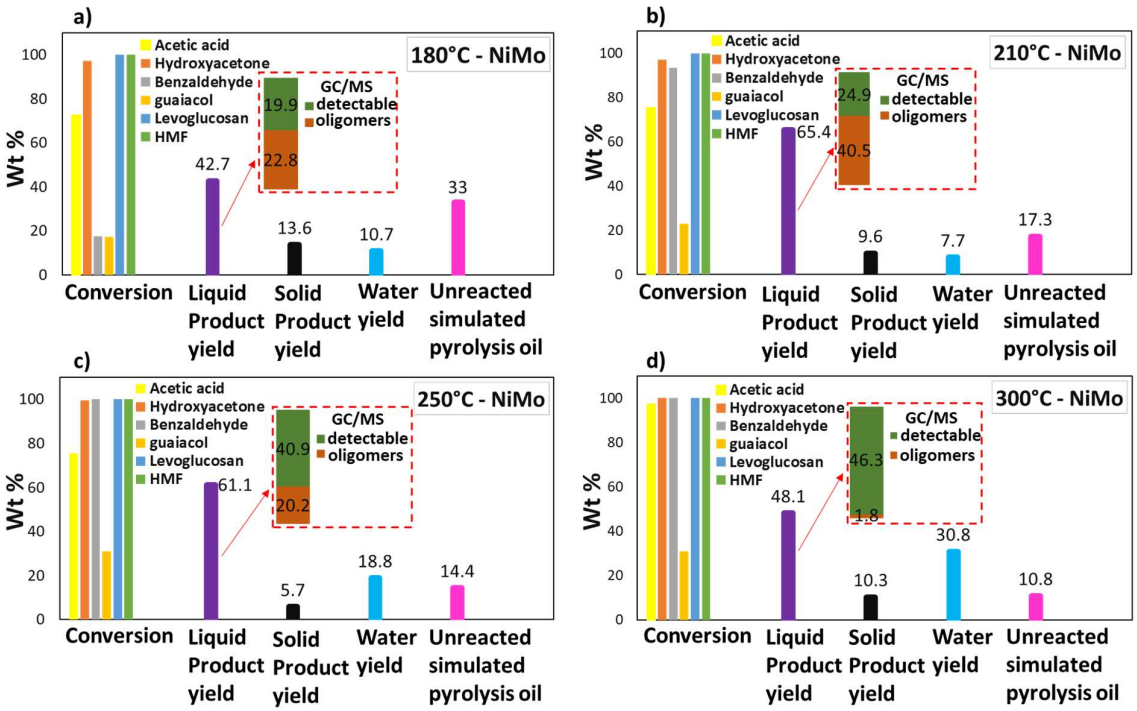

Figure 7. Effect of temperature on conversion and product yields at mild catalytic hydrotreatment, 60 bar H_2, for 4 h and 1 g $NiMo/Al_2O_3$ catalyst, a) 180°C b) 210°C c) 250°C d) 300°C

Similarly, Kadarwati *et. al* [34] reported a decreasing trend of solid content by elevating the temperature using sulfided $CoMo/Al_2O_3$ for mild hydrotreatment of real pyrolysis oil. However, an opposite trend was seen using a sulfided $NiMo/Al_2O_3$ at identical reaction conditions [34]. Various reasons can be involved in this contrasting report including: i) the different reaction conditions (3 h and 100 bar H_2); ii) the higher mass ratios of feed intake to the catalyst, which was 10 compared to 6 in our study; iii) the different ratio of oxygenated compounds present in our feedstock compared to a real pyrolysis oil used in their study. These results indicate that secondary polymerization of the intermediate fragments obtained from cracking reactions likely happened leading to enhancement in the solid content [50,51].

4.1.1.2 Liquid product compositions

The evolution of light liquid products detected by GC-MS from mild thermal and catalytic hydrotreatment of simulated pyrolysis oil using NiMo is compared in Figure 8. In the presence of the NiMo catalyst, simulated pyrolysis oil, and reactive intermediates underwent two pathways. It is evident by the formation of hydrocarbons and alcohols showing a hydrogenation path, and multiple oxygen groups compounds from condensation reactions along with subsequent secondary reactions leading to the formation of heavy oligomers in the liquid phase. Kadarwati *et. al* [52] also reported the occurrence of undesirable side reactions e.g., cross-linking

and oligomerization during pyrolysis oil stabilization using Ru/C at 250°C. By increasing the temperature, the HDO was more favored that yielded more hydrocarbons and alcohols while the yields of furanic and multiple oxygenated group compounds were reduced. Moreover, the formation of other oxygenates such as acids (mainly benzoic acid), ketones, and esters were observed at lower temperatures, and they were mostly converted at the highest temperature of 300°C (see supplementary in **paper I**). It can be explained by their conversion to favorable light products such as hydrocarbons and alcohols. This is also in line with the intense decrease in the yield of GC/MS undetectable heavy oligomers at 300°C. It suggests a strong correlation between temperature and oxygen content of the light liquid product. Light phenolic compounds and aromatic hydrocarbons such as phenol, catechol, and benzene were only seen at 250 and 300°C, inferring the occurrence of demethoxylation, and hydrogenation of guaiacol. Although at low temperatures of 180 and 210 °C, the lack of phenols among light liquid products could be assigned to participation of guaiacol on another reaction pathways such as condensation, oligomerization, and thus polymerization to form heavy compounds in accordance with the higher yield of GC-MS undetectable heavy compounds and solid obtained at these temperatures. Another interesting finding here is the complete conversion of reactive furanic compounds at elevated temperatures (300°C) mostly into light compounds where their rings were opened. This is due to the NiMo catalyst effectively catalyzing the transformation of furan. However, in the absence of the catalyst the trend was different. Two blank experiments at 180 and 300°C were carried out. The yields of all light products in the liquid phase were lower compared to catalytic experiments, except for multiple oxygen group compounds which is an indication of further condensation reactions. Moreover, almost no HDO and trace of furans were seen at 180 and 300°C during thermal hydrotreatment. The high yield of oxygenated intermediates results in the production of reactive intermediates that are key initiators for cross-polymerization reactions, which increase the solid yield (Table S2 **paper I**) [47,48]. Herein, it can be concluded that the catalyst had a valuable efficacy on the course of hydrocracking, hydrogenation, esterification, and various HDO reactions on reactive compounds/intermediates, and indeed stabilization of the simulated pyrolysis oil over the temperature range studied.

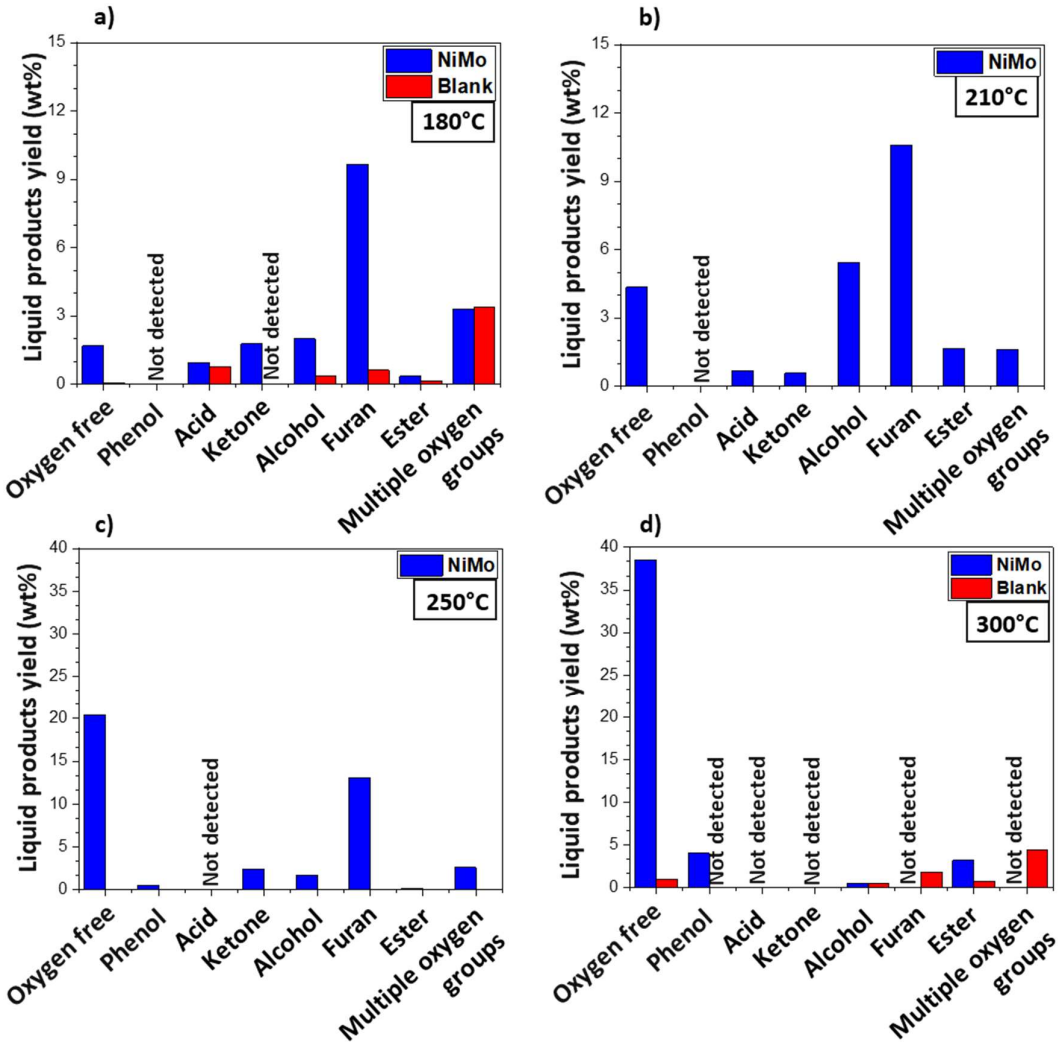

Figure 8. Light product distributions (wt%) via thermal and catalytic hydrotreatment of simulated pyrolysis oil using NiMo/Al_2O_3 catalyst. a) 180°C b) 210°C c) 250°C d) 300°C

4.1.1.3 Solids formation

The effect of temperature on solid products and char yields obtained by mild thermal and catalytic hydrotreatment of simulated pyrolysis oil is shown in Figure 9. A downward trend was found for solid yields in both catalytic and thermal hydrotreatment when temperature was increased. Although, the constructive solid-suppressing efficiency of the catalyst was obvious, particularly at the intermediate temperature of 250°C (5.7 wt%), resembles findings in literature [8]. The higher solid yield mainly at the lowest temperature, 180°C and in the absence of the catalyst (27.4 wt%), illuminates the lack of an enabling factor during thermal hydrotreatment to dissociate the hydrogen bond of H_2, allowing its atoms to bind to radicals and highly reactive oxygen-functional groups that are prone to polymerization. Therefore, there is a higher tendency to form heavy compounds at low temperatures causing higher rates of polymerization

due to further condensation reactions [43]. The solid products were extracted as soluble and insoluble solids (char) using DMSO, where the soluble fraction has a lower molecular weight. It can be observed in Figure 6b that from catalytic mild hydrotreatment, solid, and char yield showed a downward trend with elevating temperature. Furthermore, at all temperatures in the presence of NiMo catalyst, the solid is rich in the DMSO insoluble solid (char), particularly at 250°C where 91% of the solid is composed of char. Although, at 180°C the solid is composed of a soluble to insoluble mass ratio of approximately 1:1.

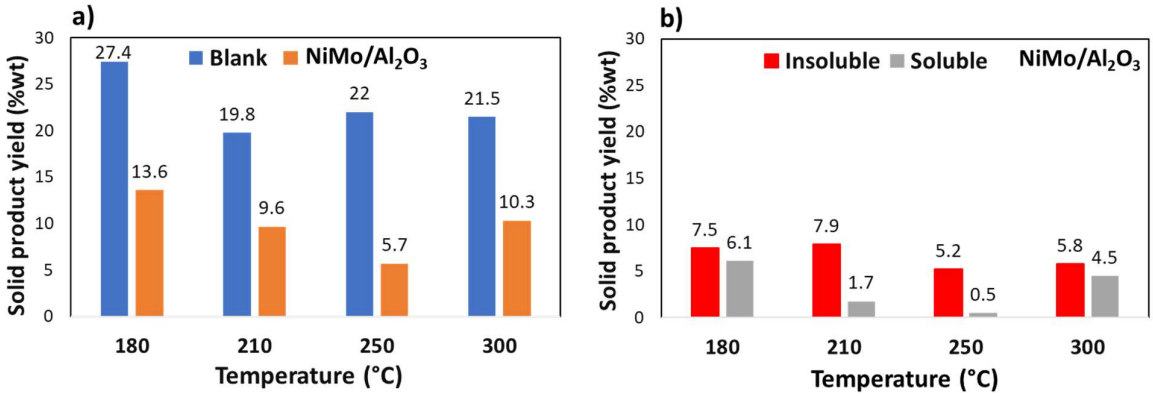

Figure 9. Effect of temperature on solid/char formation in thermal and catalytic hydrotreatment over $NiMo/Al_2O_3$ catalyst. Reactions were performed under 60 bar H_2 for 4 h. a) total solid product yield during blank and catalytic experiments. b) The yield of soluble and insoluble extracts in presence of the catalyst.

As a result, at 250°C soluble oligomers in the liquid phase were further transformed into light fractions in the liquid phase, and consequently, their further condensation to soluble polymer/solid were suppressed. Although, at the lower temperature (180°C) polymers with much higher solubility were formed giving higher yields of soluble solids.

The soluble and insoluble fractions were characterized using MALDI-TOF (scanning from 200 to 2000 m/z) and 2D-HSQC-NMR to determine the average molecular weight (M_w) and structure of the soluble fraction, and elemental analysis for composition of the insoluble solid/char, respectively. To estimate the structure of soluble solids, the average molar mass of one monomer unit from the feedstock mixture was calculated (109 Da). The wide distribution of molecular weights in the ranges 300, 500, 600, 700, 800, 900, and over 1000 m/z were assigned to trimers, pentamers, hexamers, heptamers, octamers, nonamers, and macromolecules, respectively. Table 1 presents the average M_w of the soluble solids and the C/H ratio of insoluble solids obtained from temperature variation. The average M_w of the soluble solid fractions obtained from catalytic hydrotreatment using the NiMo catalyst was higher compared to that of blank experiments (854.3 g/mol at 180°C) and reduced from 914.9

g/mol at 180°C to 522.1 g/mol at 300°C by elevating the temperature. It is an indication of the promoting effect of catalyst towards soluble polymer/solids formation instead of heavier insoluble solids. At 180°C, in the presence of the catalyst, the soluble solid was mainly composed of pentamers (551.3 m/z), heptamers (713.6 m/z), and nonamers (995.5 m/z), accompanied by macromolecules (over 1000 m/z). At higher temperatures though, no macromolecules were observed, and soluble solids are mainly made from trimers (below 500 m/z). In the absence of the catalyst though, at 180°C the soluble solid is rich in hexameric, heptameric, octameric, and nanomeric compounds. It can be concluded that both temperature and catalyst play a role on the structure of the soluble solids.

Table 1. Properties of soluble and insoluble solids obtained from the conversion of simulated pyrolysis oil at various temperatures (180-300 °C), 60 bar H_2, and reaction time t0 (at the set point temperature 180°C): 13 min reaction time, and t4: 4 h reaction time, in the absence and presence of $NiMo/Al_2O_3$ catalyst

Experiment (Time, h)	Catalyst	Temperature (°C)	Soluble solid	Insoluble solid	
			Average M_w (g/mol)	Molar ratio C/H	Yield (wt%)
t0	NiMo	180	640	0.4	3.2
t4	Blank	180	854	1	23.3
t4	NiMo	180	915	0.7	7.5
t4	NiMo	210	585	0.9	7.9
t4	NiMo	250	564	0.9	5.2
t4	NiMo	300	522	1	5.8
t4	Blank	300	-	1.1	21.5

2D-^{1}H-^{13}C-HSQC NMR was also utilized to characterize the diverse functional groups in the soluble solid fractions based on chemical shift distributions from two temperatures, 180 and 300°C (Figure 10). The detected HSQC spectrums from the soluble solids are assigned to different C-H bonds, aliphatic C-H bonds, sugars, aromatic C-H bonds, and esters which give signals at approximately δC/δH 5–55/0.5–3.8, 48–105/3–5.5, 110–125/6.2–7.5, and 122–135/6.7–7.8 ppm respectively, and similar to the literature [53–56].

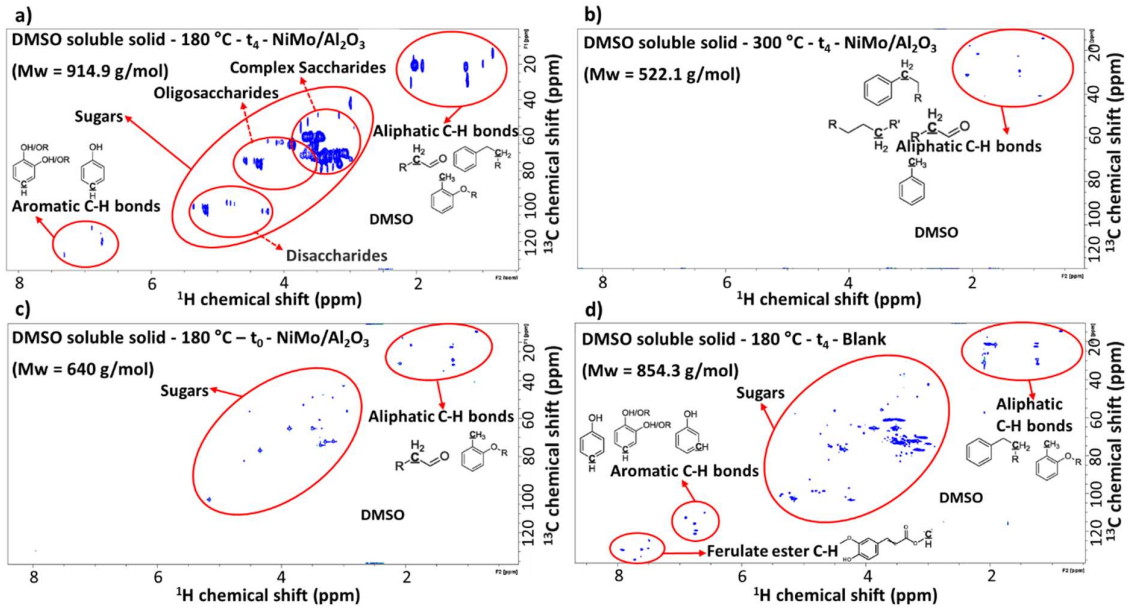

Figure 10. 2D-HSQC-NMR analysis of soluble solid obtained from mild hydrotreatment in the presence of catalyst at a) 180°C, t4, b) 300 °C, t4 c) 180°C, t0, and in the presence of catalyst (blank) d) 180°C, t4, all with 6d-DMSO as solvent, (reaction time t0 after 13 min ramp to setpoint temperature of 180°C, t4: temperature ramp and 4 h at constant temperature)

The sugar region can be classified into three regions: from (i) δC/δH 45 to 80/3-4, (ii) 65 to 90/3.5-5, (iii) 95 to 115/4.2-5.5 assigned to complex saccharides, oligosaccharides, and disaccharides, respectively [57–59]. According to Figures 10a and 10b, there is a significant difference between the structure of soluble solids obtained at 180 and 300°C where soluble solid products are composed of aliphatic, aromatic, and particularly sugars at 180°C while it is predominantly in the form of aliphatic hydrocarbons (δC/δH 5–38/0.5–2.5) at 300°C. The sugar region is in line with previous report [54] regarding NMR analysis of pyrolysis oil. These observations are proof of the occurrence of polymerization reactions mainly from sugar at 180°C, resulting in the formation of heavy sugar derivatives mainly made up of complex saccharides. These findings are in line with Kadarwati *et al.* [52] that found contributions of sugars in polymerization. However, the disappearance of sugars and aromatic C-H bonds regions at 300°C and the increase in the yield of liquid phase, indicates complete decomposition, hydrocracking, and hydrotreatment of sugar derivatives and aromatic C-H bonds [60].

In the case of insoluble solids, similar C/H ratios in the range of 1-1.1 were obtained in the absence of the catalyst at 180 and 300°C, indicating the formation of fully developed char. Similarly, a high carbon content of the insoluble polymer was reported by Sun *et. al* from thermal treatment of mixed model compounds (furan and phenols) [47]. However, in the presence of the catalyst, the C/H ratio varied and increased from 0.7 at 180°C to 1 at 300°C. Accordingly,

it seems that the catalyst promotes stabilization of reactive compounds to yield light GC detectable liquid and/or soluble solid products along with char with a lower C/H ratio in line with the GC-MS results.

4.1.2 Effect of heating-up process on simulated pyrolysis oil conversion and product yields

Among different tested temperatures (180-300°C) on mild hydrotreatment of the simulated pyrolysis oil, the highest carbon loss occurred at 180°C which is not desirable. Therefore, this temperature was highlighted so that further evaluations can be done to examine different parameters that participate in this unfavorable reaction path. The effect of reaction time and oxygenated compounds present in the simulated pyrolysis oil, as plausible influences on solids formation, has been assessed at this temperature and will be discussed in this section.

With the reactor system used, it took 13 min with the average heating ramp of 12°C.min^{-1} to reach the reaction temperature of 180°C, and samples taken after this period are labeled as t0. Two experiments focused on heating to 180°C, with and without the NiMo catalyst, were carried out and the obtained results were then compared to when the reaction was prolonged to 4 h (t4) (Figure 11).

As shown in Figure 11, in the presence of the NiMo catalyst hydroxyacetone, and levoglucosan mostly converted when the temperature rose to 180°C and there was no change in their conversion after 4 h reaction, whereas for other oxygenates such as benzaldehyde, acetic acid, and HMF, their conversions increased when prolonging the reaction time from 6, 10, and 57 wt% at the set point (t0) to 18, 73, and 100 wt% after 4 h (t4), respectively. The liquid product yield slightly decreased from t0 to t4 along with a sharp increase in the water and solid product yield. In the presence of the catalyst, water started to form in the initial 13 min with a yield of 5.8 wt%, while no water was detected at the same condition in the absence of the catalyst. Water formation at this low reaction temperature with the catalyst is primarily due to dehydration and condensation reactions but some activation of hydrogen with the NiMo metal sites causing hydrogenation and hydrodeoxygenation cannot be entirely ruled out [61]. Acid sites on the catalyst, on the other hand, can promote condensation reactions and thus yield heavy oligomers.

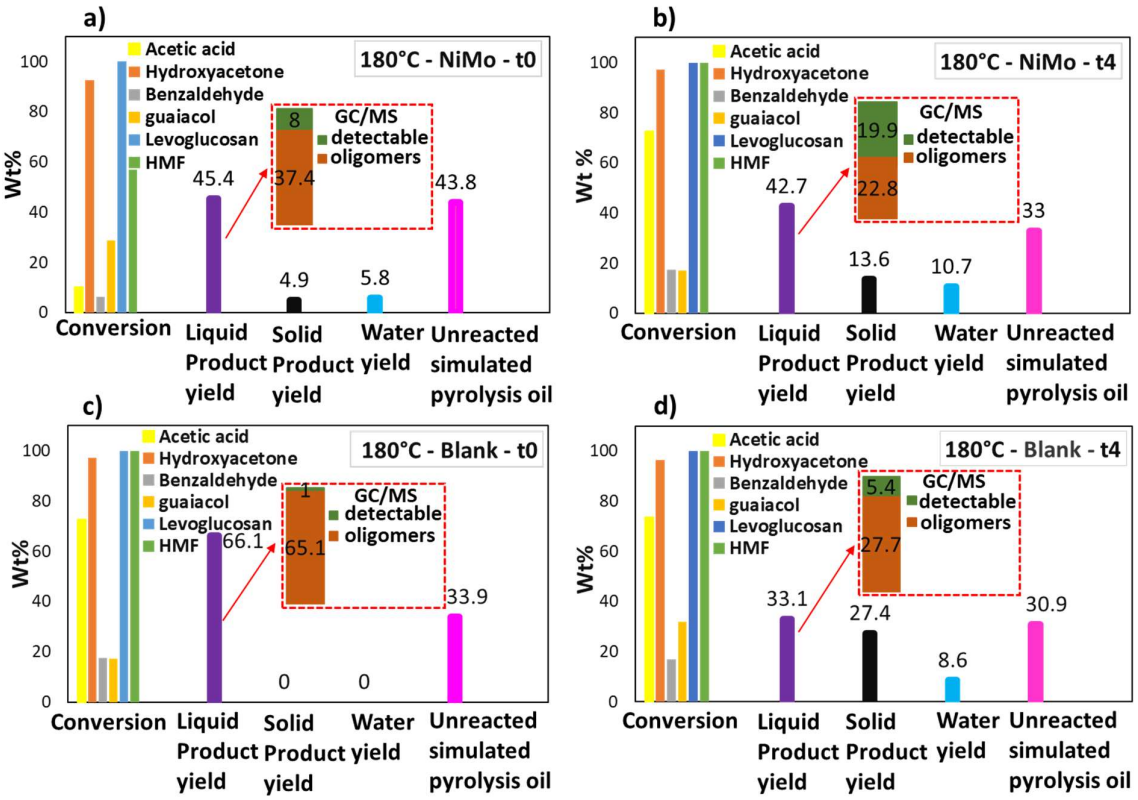

Figure 11. Effect of heating process on the conversion of oxygenated compounds in simulated pyrolysis oil and product yields (wt%). Reactions were performed by first heating at 12°C/min from room temperature to 180°C (t0), followed by 4 h at 180°C and 60 bar H_2 (t4). a) t0, b) t4 with 1 g NiMo/Al_2O_3 catalyst, c) t0 d) t4 without catalyst.

At t4 the heavy soluble oligomers partly decomposed into more light stable fractions giving the higher yield of light detectable liquid fractions which was more intense in the presence of NiMo. Surprisingly, during the heating-up process, the NiMo catalyst promoted the conversion of simulated pyrolysis oil to solids (4.9 wt%), contrary to the blank experiment with no solid formation. It suggests that polymerization, due to the acid sites of the NiMo catalyst, greatly influenced the cross-polymerization between reactive components and thereby the solid/char formation [43,62]. In addition, the NiMo catalyst was not effectively active enough to activate H_2, at a temperature below 180°C [63], to stabilize highly reactive intermediates before their polymerization and solid/char formation. Therefore, these factors should be taken into account simultaneously for barricading the formation of solids at very low temperatures [64].

Figure 12 shows the light liquid product distributions in the presence and absence of the catalyst at t0 and t4. In the catalytic experiment, a trace of hydrocarbon, and oxygenates such as phenols, acids, ketones, furans, and a high yield of multiple oxygenated compounds derived from

condensation reactions was evident during the heating-up process which reflects a slower hydrogenation activity. Subsequently, when the reaction was prolonged to 4 h, the corresponding yield of all compounds increased except the multiple oxygenated compounds which showed a 45 % drop at t4. It was also accompanied by higher degree of hydrogenation, HDO, dehydration, etc. according to the higher yields of more favorable products such as alcohols, esters, hydrocarbons, and water respectively. Moreover, a part of the heavy soluble oligomers in the liquid phase are difficult to crack even at an extended (4 h) reaction time and therefore, they were partly retained in the liquid product (Figure 12) [52].

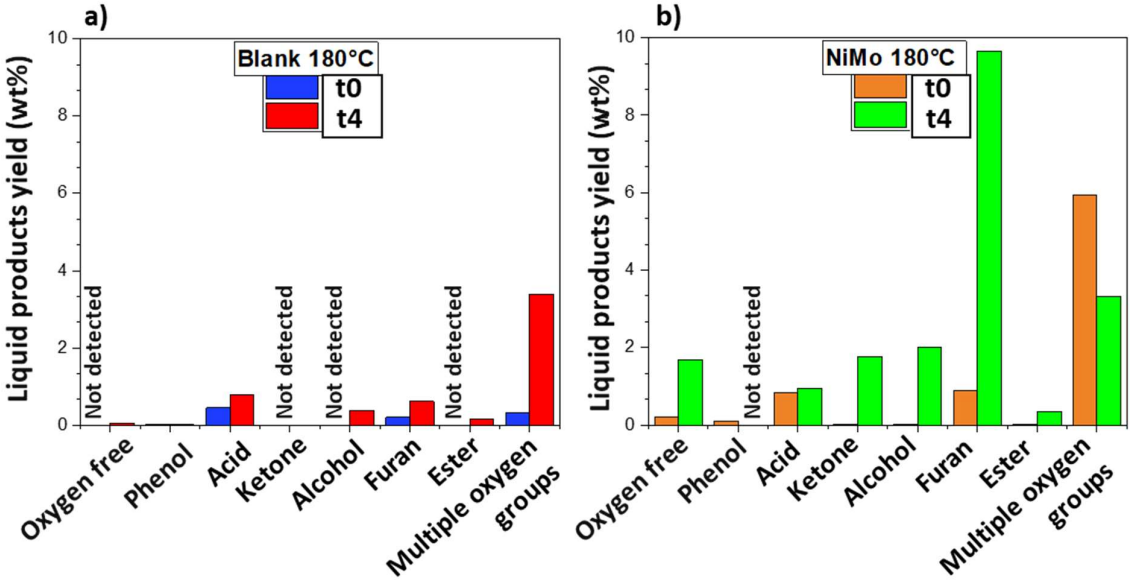

Figure 12. Light product distribution (wt%) after heating process (t0) and after subsequent 4 h reaction time (t4) for mild hydrotreatment of simulated pyrolysis oil at up to 180°C, and 60 bar H_2. a) without the catalyst, b) with the $NiMo/Al_2O_3$ catalyst

In the absence of the catalyst, higher conversion of HMF and lower yield of furans due to ring-opening reactions were seen. This might be due to reactions with other reactive intermediates that only form in the absence of the catalyst. Furthermore, at t4 without the catalyst, dehydration reactions also occurred due to either esterification or other condensation reactions [27].

A similar DMSO extraction step, explained earlier, was also performed on the solid products obtained from these experiments. Table 4 indicates that in the presence of the catalyst at t0, 65% of solids were composed of the insoluble fraction, however, prolonging the reaction time promotes soluble polymer/solid formation. But still, a higher percentage of the solid product is insoluble (55%). However, they were found to have a different nature, according to the C/H ratio depicted in Table 1. Based on the CHOS elemental analysis on the insoluble solids, a C/H ratio of 0.4 was obtained at t0 in the presence of the catalyst, indicating that the char is not fully

developed. At t4, although, the C/H ratio enhanced to 0.7, because of further polymerization a gradual enrichment of char with carbon occurred. In the absence of the catalyst, at t4 the solid was rich in the insoluble fraction (85%). Results from MALDI-TOF for the soluble solid fraction at t0 (Table 1 and supplementary in **paper I**) gave the average M_w of 640 g/mol with mainly pentameric and hexameric structures. By prolonging the reaction (t4) however, nonameric structures and even macromolecules also appeared and caused an increase in the average M_w to 916 g/mol. Figure 10c presents the NMR spectra for the soluble solids obtained during the heating process in the presence of the catalyst that features two main regions, aliphatic C-H bonds, and sugars, implying that the soluble heavy sugar and aliphatic compounds initiated solid formation even at t0. By prolonging the reaction time, apart from the rise in the intensity of these two groups, aromatic compounds were also seen (Figure 10a).

Table 2. Effect of heating process (t0) and subsequent 4 h reaction at 180°C (t4) and 60 bar H_2 on total solids and insoluble solids (char) formation

time (h)	Blank- Yield (wt%)			$NiMo/Al_2O_3$ catalyst- Yield (wt%)		
	Total solid product	Char fraction	Soluble solid fraction	Total solid product	Char fraction	Soluble solid fraction
t0	0	0	0	4.9	3.2	1.7
t4	27.4	23.3	4.1	13.6	7.5	6.1

In the absence of the catalyst at t4, approximately similar NMR spectra but with slightly lower intensity along with the ferulate ester group was seen (Figure 10d).

4.1.3 Effects of individual oxygenated groups on product yields

A series of experiments with/without catalyst at 180°C, 60 bar H_2, and 4 h reaction by removing reactants one by one, are assessed in this Section so that more light will be shed on the effect of the simulated pyrolysis oil composition on the reaction sequence.

4.1.3.1 Individual oxygenated groups and liquid product composition

Figure 13 compares product distributions comprising water, liquid, and solid products for all experiments with (on the right) and without (on the left) catalyst. By removing HMF from the simulated pyrolysis oil mixture in the presence of the catalyst, many interesting observations were obtained. Firstly, among other reactants, only hydroxyacetone conversion declined seemingly due to the stronger adsorption of other oxygenated groups and their intermediates on

the catalyst surface when it is compared to catalytic hydrotreatment containing all 6 reactants. Another possibility could be that interactions between hydroxyacetone and HMF or its products occurred that improved the conversion of hydroxyacetone. Secondly, the lack of HMF caused hydrogenation to be suppressed likely due to a decrease in the conversion of the ketone to its corresponding alcohol and thereby lower yields of hydrocarbons and alcohols were obtained. But instead, condensation and oligomerization reactions were improved, giving a higher yield of compounds with multiple oxygen groups and heavy oligomer fractions. More importantly, even in the absence of HMF in the feedstock, furanic compounds in the liquid product were found. It is because furans that can be typically produced from the catalytic dehydration of sugars [65]. In the absence of the catalyst, a similar trend as the catalytic experiment was seen with lower hydrogenation and HDO, whereas no obvious change in the conversion of other reactants was obtained. By elimination of levoglucosan from the feed mixture over the catalyst, the highest conversion of benzaldehyde and hydroxyacetone was obtained in comparison with other sets of experiments, indicating the significant effect of sugar on suppressing aldehyde and ketone conversion. Besides, the promotion of hydrogenation, HDO, and hydrocracking, a reduction in the rate of condensation, and polymerization reactions was achieved. This is evident by the satisfying yield of alcohol, esters, hydrocarbon, and light fractions as well as a reduction in the yield of multiple oxygen group compounds and heavy oligomers in the liquid phase. This could be attributed to the extra conversion of aldehydes and ketones to yield higher quantities of their corresponding alcohols and hydrocarbons. Accordingly, among catalytic experiments, the most promising result was obtained when sugar was eliminated. In the corresponding blank experiment, a higher yield of heavy oligomer compounds was gained. In addition, HMF was not fully converted probably because of the inhibitory effect of other reactants and/or their intermediates.

The most important observation from the removal of hydroxyacetone was in the absence of the catalyst, where the contribution of hydroxyacetone or its intermediates to furan ring-opening reactions during thermal hydrotreatment was evident.

The exclusion of acetic acid from the feedstock did not have a considerable effect on product distributions in both catalytic and blank experiments, although it showed lower HDO with a hydrocarbon yield of 0.3 wt% and instead a higher yield of heavy compounds at 37 wt%, particularly in the presence of the catalyst. This result complied with Xu *et. al* [43] that reported the negligible effect of organic acids like acetic acid on cross-polymerization and thus solid formation. A similar trend was obtained when guaiacol was removed, with a lower yield of hydrocarbon and a higher yield of heavy compounds with catalyst.

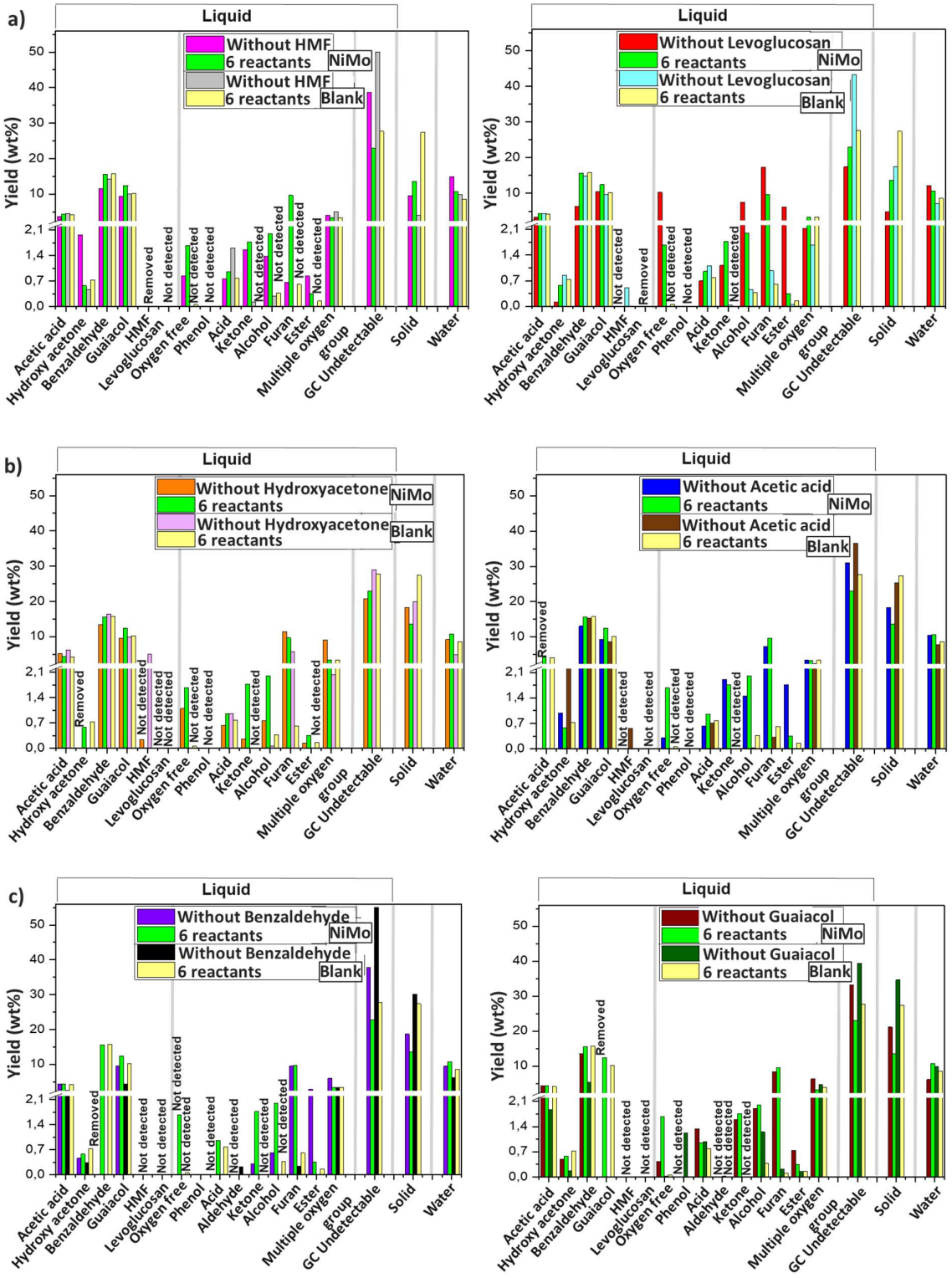

Figure 13. Effect of removing oxygenated compounds on product distributions for mild hydrotreatment of simulated pyrolysis oil at 180°C, 60 bar H_2, 4 h reaction, with and without the addition of the catalyst. Removal of a) HMF and levoglucosan, b) hydroxyacetone and acetic acid, c) benzaldehyde and guaiacol.

The remarkable effect of benzaldehyde in blank and catalytic experiments was found which is explained as follows; In the catalytic experiment by excluding benzaldehyde, no HDO occurred. Another important observation is the lack of acid products in the GC-MS results which only happened in this experiment, which might be due to the production of acid via the oxidation of benzaldehyde [66]. In the blank experiment, the highest yield of the heavy compound was seen by removing benzaldehyde, confirming the important role of benzaldehyde in inhibiting condensation and oligomerization reactions.

Among the abovementioned series of experiments in the absence of the catalyst, the solid yields decreased by the removal of hydroxyacetone, and particularly HMF, and levoglucosan. However, the opposite trend was obtained by excluding benzaldehyde and guaiacol presumably due to an increase in the content of the other reactive oxygenates such as HMF and levoglucosan, etc.

4.1.3.2 Individual oxygenated groups and solid formation

The contribution of different oxygenated groups in the simulated pyrolysis oil on the yields of solid products and their insoluble fractions is demonstrated in Figure 14. Herein, the effect of both removal of a compound and instead enhancement in the contents of other compounds should be considered for explaining the results. In the absence of the catalyst, the removal of components with less reactivity along with adding more reactive compounds caused an enhancement in solid/char content, where the minimum solid was formed by excluding the highly reactive HMF from the feedstock. One can speculate that carbon loss as a major problem during the stabilization of pyrolysis oil, mainly stems from furan because of its known potential cross-polymerization interactions with other oxygenates like sugars [43]. The high reactivity of HMF arises from the aldehyde group attached to the furan ring that activates HMF for aldol condensation reactions and the intermediates produced could continue to polymerize with other reactive oxygenated compounds to eventually form solid/char [48]. Furthermore, the opening of the furan ring confirmed by a lack of furans in the liquid phase is another reason that could promote polymerization and thus the formation of solids. In the catalytic experiments, on the other hand, the removal of reactive levoglucosan, showed the greatest effect on the diminishment of solid content. This is likely owing to the high reactivity of levoglucosan over the acidic $NiMo/Al_2O_3$ catalyst that is hydrolyzed to form glucose followed by its further degradation to furans, which remarkably contributes to the formation of solid/char [67,68]. Therefore, furans could be produced from both levoglucosan, and HMF over the catalyst.

It is noteworthy to mention that, comparing all experiments, the lowest carbon loss as solids was obtained in the absence of the catalyst, when HMF was eliminated and the solid mainly consisted of the soluble fraction similar to when hydroxyacetone was removed. With the addition of the catalyst though, the solid product showed a different composition comprised of mainly DMSO soluble solids (87%) while for other experiments solids were largely made up of insoluble solid/char (Figure 14b). This suggests that the solubility of the polymers/solids formed is a function of polymerization reactions, which is affected by various oxygenated compounds.

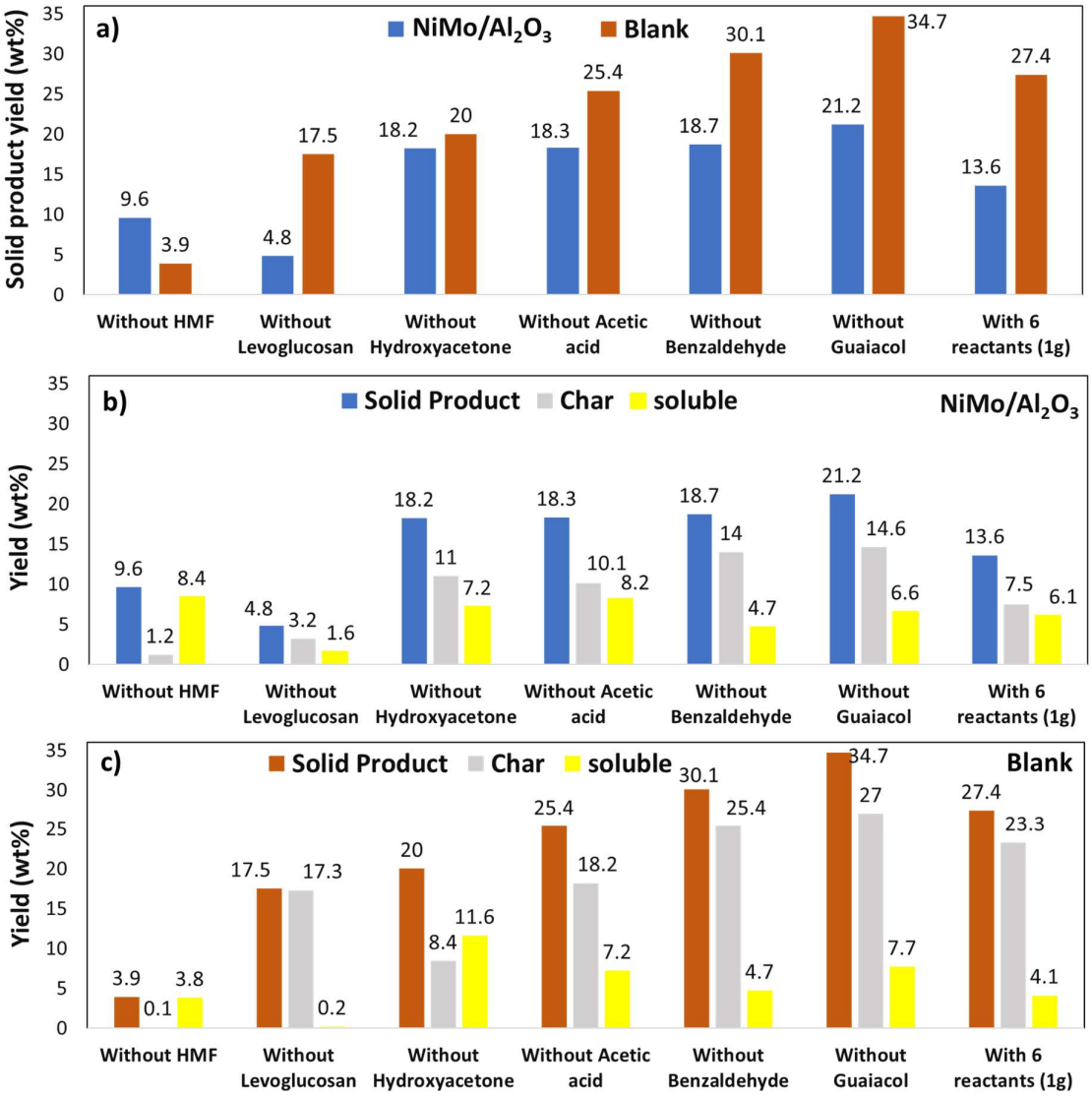

Figure 14. Effect of components excluded from feedstock on solid product yield in experiments performed at 180°C, under 60 bar of H_2 for 4h. Solid product yield during blank and catalytic experiments (a). Yield of soluble and insoluble extracts in presence of the catalyst (b), and in the absence of the catalyst (c).

Table 3 shows the effect of removing the oxygenated compounds present in the simulated pyrolysis oil on properties of both the soluble and insoluble solids. Elimination of HMF from catalytic experiment gave mainly soluble solids with the highest average M_w (1187 g/mol) and an extensive distribution of molecular weights comprising hexamers, and up to macromolecules. On the other hand, in the same experiment but without the catalyst a lower average Mw of 729 g/mol from MALDI-TOF analysis was obtained. The different Mw of these two soluble solids is due to the influence of the catalyst on repressing the transformation of soluble polymer/solids into heavier insoluble polymer/solids.

Table 3. Properties of soluble and insoluble solids obtained from the removal of individual compounds for experiments at 180°C, 60 bar H_2, and reaction time t4: 4 h in the absence and presence of the $NiMo/Al_2O_3$ catalyst.

Component removed	Catalyst	Temperature (°C)	Soluble solid	Insoluble solid	
			Average M_w (g/mol)	Molar ratio C/H	Yield (wt%)
HMF	NiMo	180	1187	0.2	1.2
HMF	Blank	180	729	-	0.1
Levoglucosan	NiMo	180	647	0.5	3.2
Levoglucosan	Blank	180	590	1.1	17.3
Hydroxyacetone	NiMo	180	949	0.8	11
Hydroxyacetone	Blank	180	1059	0.9	8.4
Acetic acid	NiMo	180	801	0.8	10.1
Acetic acid	Blank	180	837	1	18.2
Benzaldehyde	NiMo	180	896	0.8	14
Benzaldehyde	Blank	180	622	1	25.4
Guaiacol	NiMo	180	762	0.9	14.6
Guaiacol	Blank	180	912	0.9	27

On the other hand, the removal of levoglucosan in the presence of the catalyst resulted in soluble solids with different structures. They were mainly composed of pentameric and hexameric structures. Heavier structures such as macro molecules were not detected and thus a lower average M_w of 647 g/mol was obtained. This is an indication of the lower tendency of other oxygenates and/or reactive intermediates to be polymerized due to a lower propensity for cross-

polymerization occurring between sugar and other oxygenates [43] when the sugar was absent. This is comparable to the GC data where a lower yield of the heavy oligomers was achieved in the liquid phase when the sugar was omitted from the pyrolysis oil. The removal of other oxygenated compounds in both catalytic and blank experiments though, had little effect on the soluble solid structure.

In the case of insoluble solids, to understand their nature, the C/H molar ratio was measured (Table 3). The structure of the insoluble solids was principally affected by sugar and furan as the lowest C/H molar ratio of ≤ 0.5 was obtained by the removal of these two groups in the catalytic experiments caused the insoluble solids to be free of fully developed char. Removal of other less reactive oxygenated compounds in the presence of NiMo catalyst, gave an increase in the C/H molar ratio in the region of 0.9, suggesting the formation of more fully developed char. In the absence of the catalyst, the C/H molar ratio was in the range of 0.8 to 1.1 for insoluble solids, indicating the char was well developed

4.1.4 Reaction pathway for mild hydrotreatment

The various reaction pathways occurring during mild hydrotreatment of simulated pyrolysis oil are presented in Scheme 1, which includes:

i) Hydrogenation of oxygenates to yield light and more stable oxygenates such as alcohols as well as hydrocarbons via HDO which are more favored at elevated temperatures and in the presence of the catalyst.

ii) Condensation reactions between reactive compounds and intermediates which mainly occur at lower temperatures primarily between furans, sugars, and aldehydes and thereby act as an initiator for the formation of heavy oligomers.

iii) Oligomerization and subsequently polymerization reactions causing the formation of heavy fractions in liquid and solid states. These reactions occur in the absence of the catalyst and further at lower temperatures mainly originated from HMF and levoglucosan conversions.

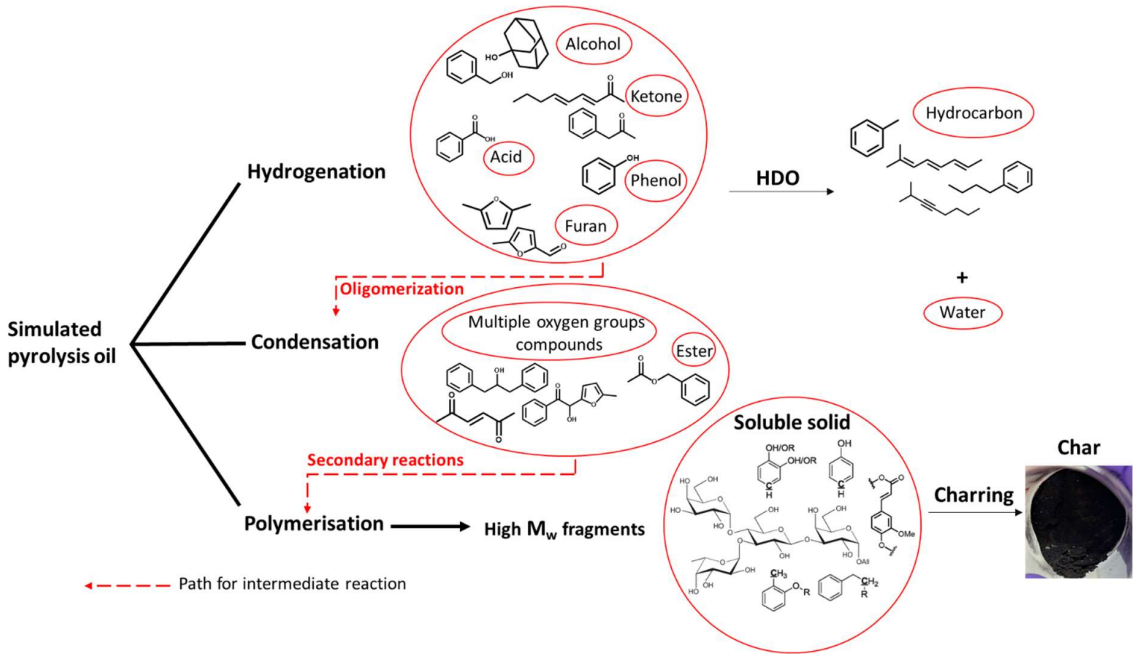

Scheme 1. Proposed main reaction pathways during mild catalytic hydrotreatment of simulated pyrolysis oil

4.2 The effect of catalyst composition on the stabilization process

Various alumina-supported noble metals (Rh, Pt, and Pd) and Re catalysts were assessed in **paper II** for stabilization of the same simulated pyrolysis oil applied in the first study at mild conditions to examine the effect of these catalysts on stabilization of the various oxygenated compounds at 180°C, 60 bar H_2 over 4 h residence time. Their performance was compared with $NiMo/Al_2O_3$ and blank, without the catalyst. The effect of Pd loading on the quality and distribution of products was then further evaluated. The efficiency of each metal was evaluated by analysis of the liquid product via GC/MS and Karl-Fischer. A solid product extraction to DMSO soluble and insoluble fractions was done to examine the degree of polymerization. A deeper understanding of the transformations that occur between these fractions using different catalysts can be acquired by further analyses, such as elemental analysis, TGA, and 2D-HSQC-NMR that are ongoing. Furthermore, all catalysts will be characterized by SEM and TEM to measure particle size distributions and gain a better understanding of their behavior.

4.2.1 Simulated pyrolysis oil conversion and product yields

Figure 15 shows the conversion of different oxygenates, and product distributions over various catalysts (Rh/Al_2O_3, Pt/Al_2O_3, Pd/Al_2O_3, and $NiMo/Al_2O_3$) and in the absence of a catalyst (blank). HMF, levoglucosan, and hydroxyacetone were found to be fully converted in all experiments, while the conversion of other oxygenates, benzaldehyde, guaiacol, and acetic acid

fluctuated. In the case of benzaldehyde, the highest conversion (~ 70%) was obtained by Pd/Al_2O_3, followed by about 40% using Pt/Al_2O_3 and Rh/Al_2O_3 catalysts. However, it was below 40% in the experiments using Re/Al_2O_3, and $NiMo/Al_2O_3$ and reached the lowest conversion in the absence of the catalyst (below 20%). Opposite to benzaldehyde conversion, the lowest conversion of guaiacol (~ 20%) was obtained in the presence of $NiMo/Al_2O_3$, Pt/Al_2O_3, and Rh/Al_2O_3 catalysts, whereas its conversion reached about 30 % using $Pd//Al_2O_3$, Re/Al_2O_3, and blank experiment. Compared to benzaldehyde and guaiacol, acetic acid showed higher conversion and its conversion reached about 80% in the presence of Rh/Al_2O_3, Pd/Al_2O_3, and Pt/Al_2O_3 catalysts but was below 80 % for the blank experiment as well as for $NiMo/Al_2O_3$, and Re/Al_2O_3. Generally, the minimum yield of unreacted simulated pyrolysis oil was seen using Pd (18.4 wt%).

Liquid product yields, determined from mass balances, were compared over the various catalysts as well as blank experiment, and Pd was found to have a promising liquid yield (Figure 15). The liquid yields decreased in the following order for the catalysts: Pd/Al_2O_3 (65.9%) > Rh/Al_2O_3 (51.2%) > Pt/Al_2O_3 (48.5%) > $NiMo/Al_2O_3$ (42.1%) > blank (41.7%) > Re/Al_2O_3 (31.7%).

The liquid product obtained from all experiments contained both a light fraction (GC/MS detectable) and heavy oligomeric compounds. Comparing all experiments, although liquid products were rich in heavy oligomers, the yields of low molecular weight compounds in the liquid products using Pd/Al_2O_3, Rh/Al_2O_3, and $NiMo/Al_2O_3$ were higher, indicating that the simulated pyrolysis oil underwent less condensation and oligomerization reactions with these catalysts. In contrast, in the absence of the catalyst as well as in the presence of Pt/Al_2O_3 and particularly Re/Al_2O_3(Figure 15), the yields of heavy oligomers were higher. This is in accordance with their high solid yields suggesting these soluble heavy oligomers undergo secondary reactions to form solid precursors.

The measured water yield from the liquid product showed noticeable variations with and without catalysts, ranging from 3.9 to 12.4 wt%. An important reaction causing water formation is hydrodeoxygenation (HDO) [69] during hydrotreatment of pyrolysis oils. However, the various dehydration and condensation reactions occurring between oxygenates also contribute to the formation of water. The highest water contents were found in the presence of Pd and NiMo 12.4 and 10.7 wt%, where also oxygen free compounds were formed (as will be discussed in Section 4.2.2) suggesting that HDO was an important reaction over these catalysts. Oppositely, the water yield using Pt was very low (3.9 wt%) while it slightly increased to 7.1 and 6.9 when Re and Rh were applied respectively, likely because of condensation reactions. This implies the

effect of metals on promoting/suppressing dehydration reactions. Similarly, Oh *et al.* [29] reported various water contents produced from hydrotreatment of pyrolysis oil in the presence of Pt and Ru over carbon.

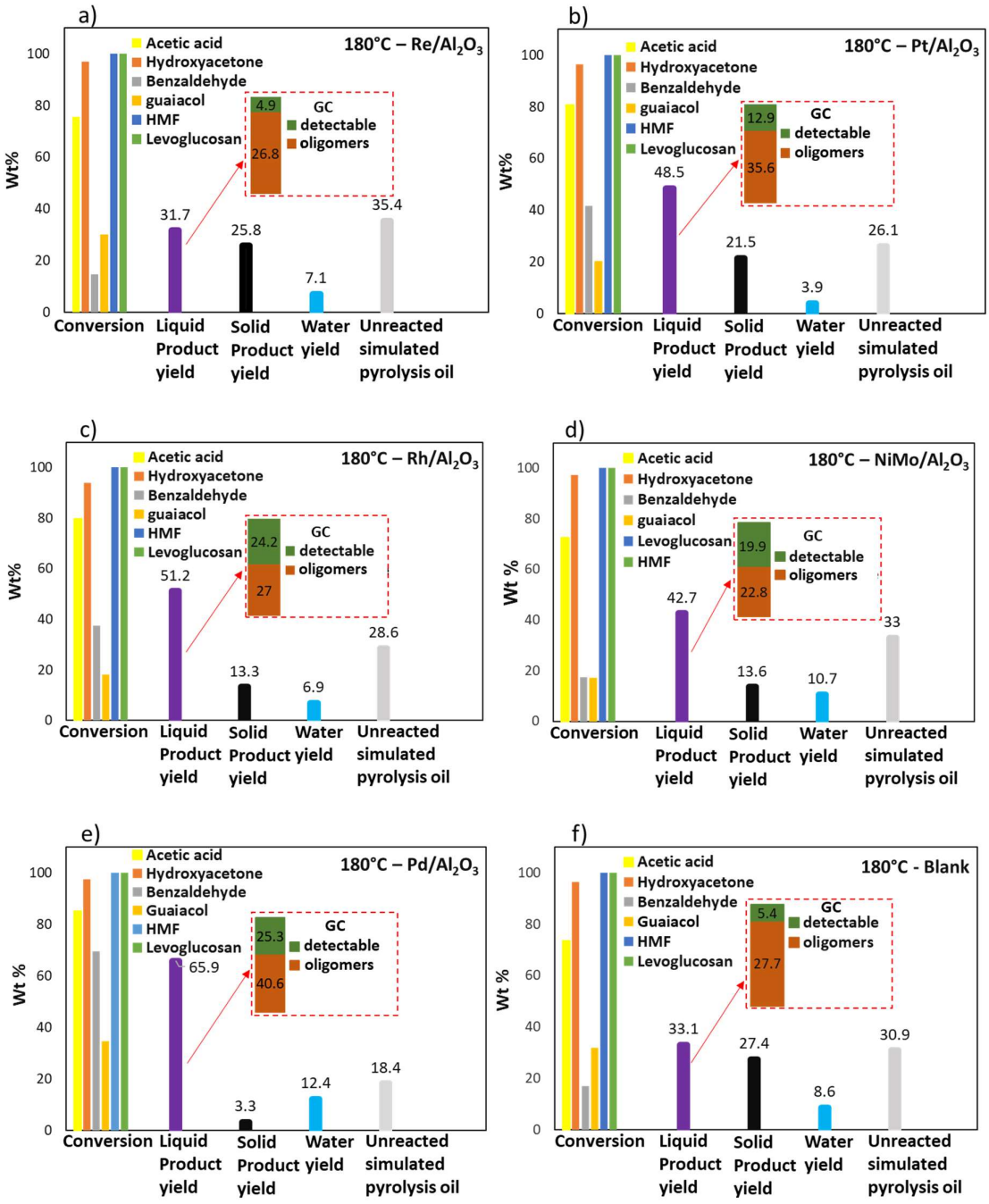

Figure 15. Conversion of oxygenated compounds in simulated pyrolysis oil, and yields of liquid and solid products, water, and unreacted simulated pyrolysis oil (wt%) over 1 g alumina supported a) 1.9% Re, b) 1.7% Pt, c) 1.8% Rh, d) 3.6% Ni, 13.2% Mo NiMo, e) 1.8% Pd catalysts and f) blank experiment. Reaction conditions: 180°C and 60 bar H_2 for 4 h. Yields of oligomers determined from mass balance.

The formation of solids derived from condensation and subsequent polymerization was observed in the presence and absence of catalysts, although it was varied depending on the type of metal loaded on the alumina-supported catalysts. It was severe for the blank experiment, without the catalyst (27.4 wt%). Coke deposition as a result of the formation of high M_w compounds from polymerization reactions, can cover catalysts' active sites and thus affect catalyst activity. Apparently, Re is more favorable for polymerization than hydrogenation causing quicker blockage of active sites by heavy compounds and consequently reducing the catalyst activity significantly. This explanation is in line with high yield of heavy oligomers in the liquid phase as well as high amount of solid formed.

4.2.2 Liquid product distribution

The composition of light compounds in the liquid products obtained from thermal and catalytic hydrotreatment were examined by GC/MS. The yield of various groups of oxygenates and deoxygenated compounds was studied for each catalyst and blank, without catalyst (Figure 16). The multi-oxygenated compounds detected in all experiments were derived mainly from sugars, furans, and aldehydes, whereas deoxygenated compounds were mainly toluene. Based on the identified products via GC/MS, the lowest yield of light compounds was found over Re which were mainly composed of multi-oxygenated compounds, while no phenols, ketones, acids, and oxygen free compounds were observed. In the first study furans and sugars were found to be the reactants with very high reactivity and tendency for cross-linking with other intermediates such as phenols and thus causing polymerization [70]. A trace of light furans ($\leq$ 0.5 wt%), and instead a high yield of oligomers was seen using Re. Therefore, it is clear that HMF contributed to the formation of heavy compounds through polymerization and ring-opening reactions, suggesting this catalyst could not stabilize these highly reactive oxygenates. Similarly, in the blank experiment, a low amount of light compounds but instead more heavy oligomers were formed which should be precursors for forming polymers/solids. However, the composition of light liquid fraction in the absence of the catalyst was slightly different, with higher yields of acids and multi-oxygenated compounds.

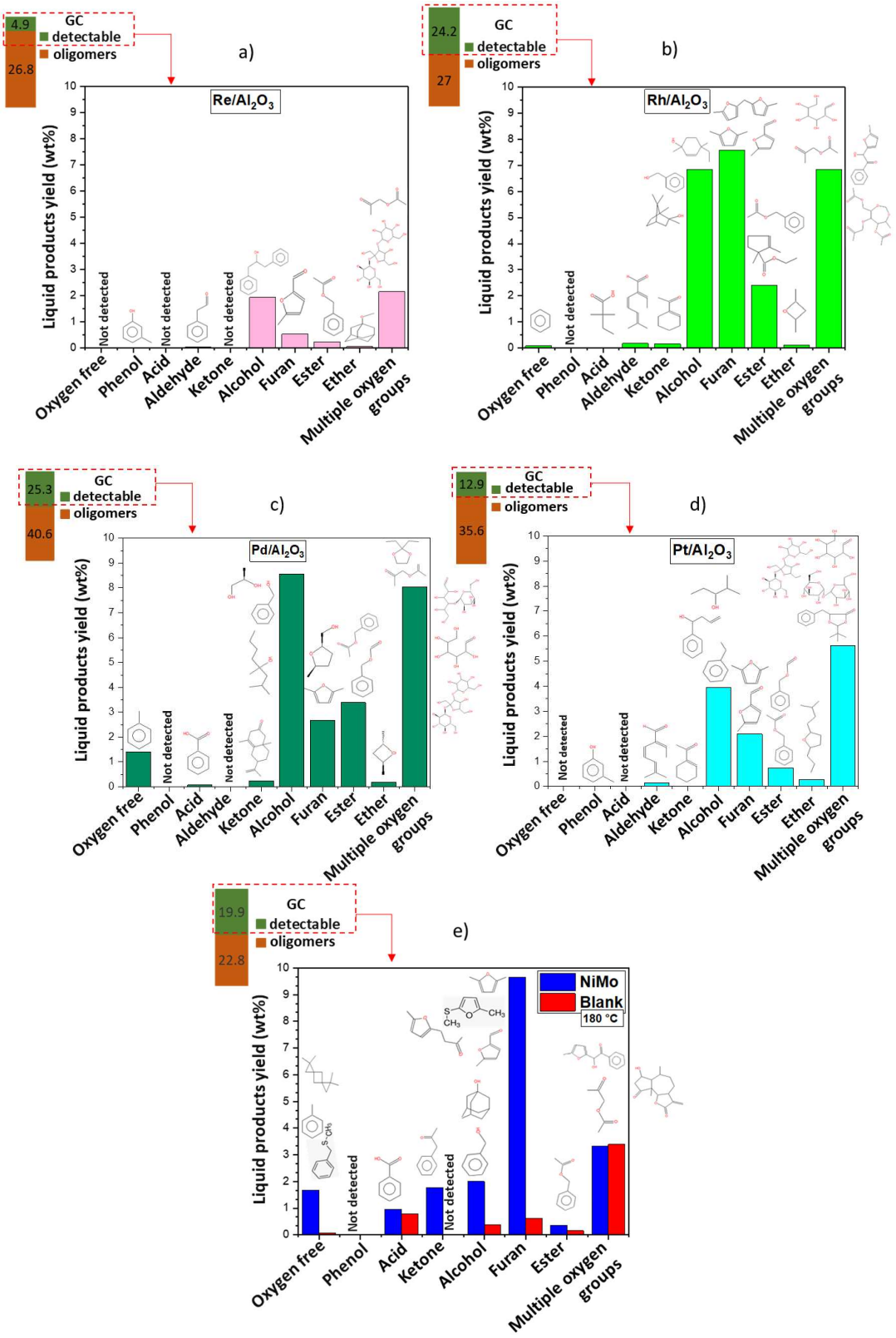

Figure 16. Distribution of the light liquid products (wt%) produced by thermal and catalytic hydrotreatment of simulated pyrolysis oil using a) Re/Al_2O_3, b) Rh/Al_2O_3, c) Pd/Al_2O_3, d) Pt/Al_2O_3 (a-d 2 wt% metal), e) blank and $NiMo/Al_2O_3$ catalysts at 180°C and 60 bar H_2 for 4 h.

Compared to the above-mentioned metals, Pt was slightly better in stabilization of the simulated pyrolysis oil with a more than double yield of the light liquid fraction (12.9 wt%), consisting of mainly alcohols, furans, and multi-oxygenated compounds (Figure 16). It implies that Pt/Al_2O_3 was more able to stabilize furanic compounds, and thus the rate of furan ring-opening and polymerization reactions declined. Although, no deoxygenated and light oxygenates such as phenols, acids, and ketones were observed. Our result is in line with observations by Runnebaum *et al.* that reported the occurrence of furan ring-opening reactions during mild hydrotreatment of furan over a Pt/Al_2O_3 catalyst.

Interestingly, the conventional $NiMo/Al_2O_3$ catalyst showed a better performance compared to previously discussed noble metals. However, it should be mentioned that the metal loading was significantly higher for this catalyst (3.6 and 13.2% for Ni and Mo respectively). With NiMo, the composition of the liquid product significantly changed with an increase in the yields of light hydrotreated oxygenates, alcohols (2 wt%), ketones (1.8 wt%), and particularly furans (9.7 wt%) as well as a higher yield of water but also the highest amount of acid products and formation of deoxygenated compounds via probably HDO of benzaldehyde. This is in line with previous literature reporting that sulfided $NiMo/Al_2O_3$ catalysts favour direct HDO [71,72]. In addition, the rate of undesirable reactions (oligomerization and polymerization) reduced and instead hydrocracking and HDO increased. The Rh/Al_2O_3 was comparable to NiMo in terms of solid yield, however, the quality of the corresponding light liquid products was different. Rh showed liquid product with higher yield of alcohols, esters, and multi-oxygenated compounds, but very low yield of oxygen free compounds.

For Pd, the quality of the liquid product significantly improved as oligomerization and polymerization reactions were suppressed remarkably. However, the liquid products obtained from all experiments were still rich in the heavy oligomer fraction. Accordingly, the soluble oligomers need to be analyzed via GPC and 2D-HSQC-NMR to further elucidate the effect of the metals on the content of the heavy liquid products. In the presence of Pd, some benzaldehyde undergoes HDO reactions to yield toluene (1.5 wt%), similar to Rh. Furthermore, Pd could enhance the rate of dehydration as well as the yield of favourable stable alcohols (8.6 wt%), esters (3.4 wt%), multi-oxygenated compounds (8 wt%) and more importantly ring hydrogenated furans with high stability all increased. Therefore, it is evident from the GC/MS results that HMF and its reactive intermediates were stabilized to a large extent using Pd, in line with the least carbon loss as solids. Overall, Pd can promote hydrocracking reactions and

hydrogenate oxygenates with high efficiency for esterification reactions and stabilizing furans. However, NiMo-S/Al_2O_3 like Rh/Al_2O_3 was fairly good in hydrocracking as well as catalyzing the transformation of many of the reactive compounds, however, this was not the case for furans. In addition, the production of deoxygenated compounds was more favored using NiMo. Furthermore, Pt and particularly Re showed weak performance for suppressing condensation, oligomerization, and polymerization reactions.

4.2.3 Solid product

Solid formation lowers the carbon conversion efficiency of simulated pyrolysis oil, as well as causing catalyst deactivation. Figure 17 compares the effect of different alumina-supported catalysts to that in the absence of the catalyst on solid formation during mild hydrotreatment. It is obvious that among applied catalysts, Re was the weakest in suppressing heavy polymers/solids formation with a total solid yield of 25.8 wt%, slightly lower than when the catalyst was absent (27.4 wt%). However, carbon loss was less for the other catalysts in the following order: Pt (21.5 wt%) > NiMo (13.6 wt%) > Rh (13.3 wt%) > Pd (3.3 wt%).

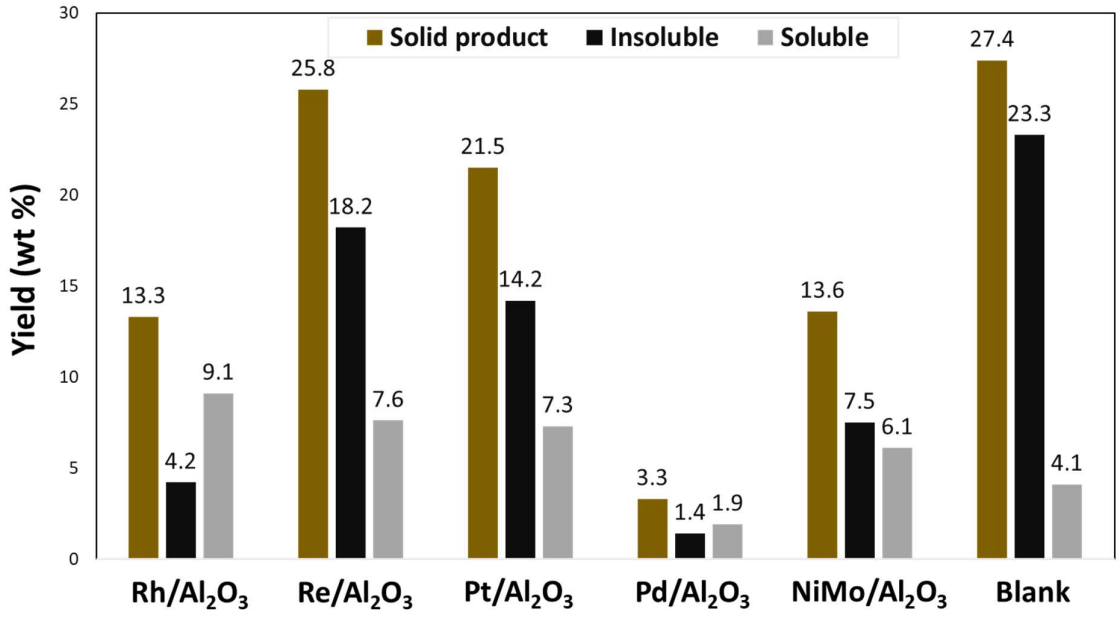

Figure 17. Solid contents (wt%) and distribution of DMSO soluble and insoluble fractions obtained from mild hydrotreatment of simulated pyrolysis oil using various catalysts.

The supremacy of the Pd catalyst in terms of reducing the solid yield (3.3 wt%) is obvious. The low solid formation using Pd implies its inhibitory effect on the transformation of heavy oligomers, undetectable by GC/MS, into heavy polymers and, thus into solids. Rh/Al_2O_3 was also fairly good at stabilizing reactive compounds/intermediates because it reduced the solid

product in about half compared to Re, and Pt metals. Interestingly, in this regard, the performance of the conventional NiMo/Al_2O_3 was comparable to Rh/Al_2O_3 and even better than that of using Pt/Al_2O_3. However, according to the literature [24], pre-sulfided NiMo catalysts were less active in suppressing solids compared to noble metals (Pd, and Pt) during hydrotreatment of real pyrolysis oil. They suggest that this may be due to the absence of a sulfiding agent in the feed to keep the catalyst active during the reaction [24]. In another study done by Lin *et al.* [73], Rh showed better activity for hydrotreatment of guaiacol, compared to NiMo in agreement with the observation in our study. As a result, the solid content formed is strongly related to the type of metal in the catalyst.

As in **paper I**, the solid products were extracted into DMSO soluble and insoluble fractions to determine the degree of polymerization of the solid. The solid product formed from thermal hydrotreatment was rich in the heavy insoluble fraction, accounting for 85% of the total solid (Figure 17). Similarly, in the case of Re, Pt, and NiMo catalysts, solids mainly contained the insoluble fraction, but with lower ratio, which suggests that the soluble polymers with lower molecular weight underwent further polymerization to yield the heavier insoluble fractions. However, in the presence of Rh and Pd, the nature of solids was significantly different, because the soluble fractions were more dominant. This is an indication of the inhibitory effect of Rh and Pd on the further conversion of soluble solids/polymers into heavier insoluble solids/polymers. As a result, the transformation of soluble polymers/solids into heavier insoluble polymers/solids were more favored using NiMo, Re, and Pt, whereas Rh and Pd more selectively yielded soluble polymers/solids instead, under the same reaction conditions. The product distributions obtained during stabilization of the simulated pyrolysis oil using the different alumina-supported catalysts along with the composition of the liquid product will be further explained by a proposed reaction network.

4.2.4 Effect of Pd loading on product distribution

Among the different examined catalysts, Pd/Al_2O_3 was highlighted as the superior catalyst with the highest degree of stabilization and minimal carbon loss as solids. Therefore, this metal was selected for further evaluation by studying the effect of Pd loading over alumina on product distributions and determining what could be near its optimum loading by comparing two Pd/Al_2O_3 samples with 1.8 and 3.9 wt% Pd, respectively. Table 3 shows the effects of the Pd loading of the Pd/Al_2O_3 catalyst on the conversion of oxygenates and the yield of products obtained from the mild hydrotreatment of simulated pyrolysis oil at 180°C, 60 bar H_2 after a 4 h reaction period.

Table 3. Conversion of simulated pyrolysis oil and distribution of the resulting products with two different Pd loadings at 180°C and 60 bar H_2 for 4 h. *Determined from mass balance.

		Reactants and Products		Pd loading wt%			
				1.8		3.9	
Wt%	Conversion	Acetic acid		85.4		79.4	
		Hydroxyacetone		97.5		100	
		Benzaldehyde		69.7		93.3	
		Guaiacol		34.7		21	
		HMF		100		100	
		Levoglucosan		100		100	
	Yield	Liquid product		65.9		69	
		GC detectable	GC undetectable	25.3	40.6	37.8	31.3
		Solid product		3.3		7.7	
		DMSO soluble	DMSO insoluble	1.9	1.4	5.5	2.2
		Water		12.4 ± 0.2		6.8 ± 0.2	
		Unreacted simulated pyrolysis oil		18.4		16.4	

At higher Pd loading (3.9 wt%) the conversion of different oxygenates only slightly changed, except benzaldehyde that was enhanced to 93 %. It was also observed that the yields of liquid and solid products by increasing the Pd loading were enhanced from 65.9% and 1.8 wt% to 69% and 3.9 wt% respectively, while the water yield was reduced from 12.4% to 6.8%. More importantly, the liquid product was mainly composed of light fractions at higher Pd loading, unlike the corresponding liquid product at low Pd loading in which heavy oligomers were dominant. Furthermore, at higher Pd loading, along with increasing the solid yield, its composition also changed to a higher percent of the DMSO soluble fraction (> 70%) among solids. It can be concluded that too high Pd loading renders further formation of soluble polymers accompanied by larger amounts of solids overall.

The composition of the light liquid fraction obtained from the catalysts with different Pd loading were evaluated by GC/MS. Figure 18 illustrates the evolution of groups of light products where the group termed “other oxygenates’’ includes aldehydes, ketones, ethers, and phenols.

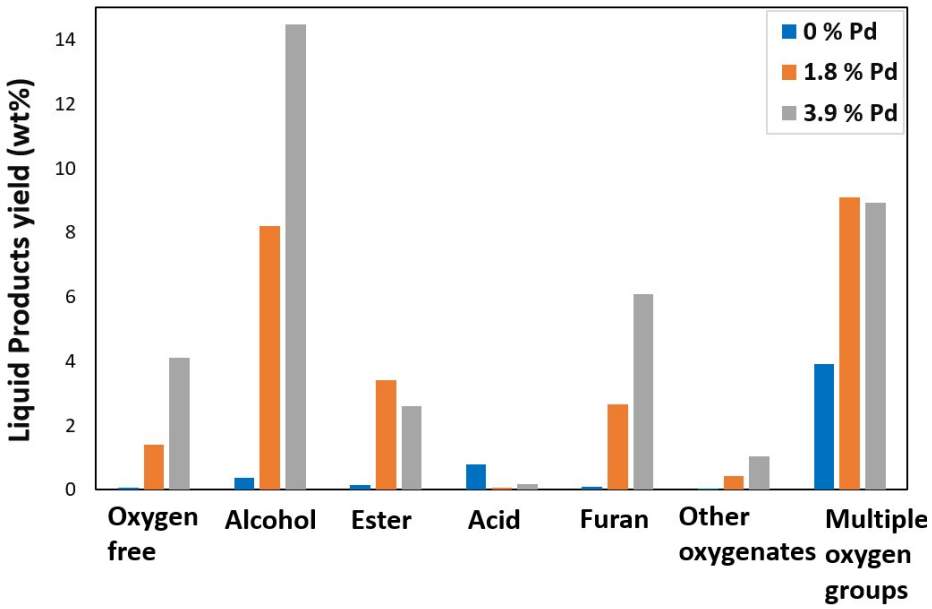

Figure 18. Effects of Pd loadings on the distribution of light liquid compounds during the stabilization of simulated pyrolysis oil using 1.8 and 3.9 wt% Pd. Reaction conditions: T= 180°C, P= 60 bar H_2 and 4h. The experimental points for 0 wt% metal loading is result of an experiment without the catalyst (blank).

According to the GC/MS results, the yields of alcohols, light stable furans (hydrogenated furan ring), and oxygen free compounds were enhanced by increasing the Pd loading, indicating that the amount of active Pd needed to be sufficiently high to promote further hydrogenation, and deoxygenation (HDO) reactions. However, the yield of esters decreased while the yield of multiple oxygenated compounds remained almost constant at higher Pd loading. This is possibly due to further oligomerization of the formed multiple oxygen compounds to form solids, which is higher for the 3.9 wt% Pd/Al_2O_3 sample. Moreover, higher conversion of benzaldehyde in the presence of 3.9 wt% Pd/Al_2O_3 eventually leads to the formation of reactive -cyclohexen-1-carboxaldehyde, 3-methyl- (CCM) and traces of α-Santonin (see Table S1 in **paper II**). These partially hydrogenated intermediates probably originating from a partial reduction of benzaldehyde, have a high tendency to further condense with highly reactive intermediates such as furans and multiple oxygenated group compounds or soluble oligomers, and with further polymerization, this promotes solid formation [42,43,47]. This observation suggests that 3.9 wt% Pd loading was not sufficient to effectively hydrogenate the aromatic ring of the benzaldehyde derivative (CCM). Therefore, it is reasonable to conclude that the extent of metal loading could affect both distribution and composition of products. The increased palladium loading resulted in a slight increase in bio-liquid yield and quality, however, the solid content also increased. However, previous studies on stabilization of real pyrolysis oil using various

metal loadings, reported different trends [25,38]. According to the observations by Zanuttili *et al.* [38] on mild hydrotreatment of m-cresol using a Pt/Al_2O_3 catalyst at 300°C and atmospheric pressure of Hydrogen, by increasing Pt loadings from 0.05 to 0.5 wt% the solid content increased in line with our observation. However, by further increase of Pt loading from 0.5 to 1.7 wt%, the reduction in oxygenated compounds was accompanied by a lower solid yield [38]. In another study on mild hydrotreatment of pyrolysis oil using a Pd/C catalyst at 230°C, the results were opposite where solid yield decreased and the quality of liquid product improved to a higher yield of deoxygenated compounds by increasing the Pd loading from 5 to 10 wt% [25]. In our experiment if only insoluble solids are considered the amounts are quite similar between the two palladium loadings where a significantly lower temperature (180°C) was performed compared to the mentioned two studies (300 and 230°C), which could explain the differing trends.

4.2.5 Reaction pathway

During stabilization of simulated pyrolysis oil over various metal alumina-supported catalysts at 180°C, several favorable and unfavorable reactions occur simultaneously. However, the intermediates and products could be varied depending on the metal type and its loading. Based on the identified products/intermediates via GC/MS, a suggested reaction network is shown in Scheme 2, in which the light liquid compounds including deoxygenated and oxygenated monomers with different functional groups, as well as multi-oxygenated compounds derived from condensation reactions, are depicted in the green box. These condensed compounds along with reactive intermediates undergo further oligomerization which leads to the formation of higher molecular weight soluble oligomers in the liquid phase and thereafter upon further cross-linking gives polymer/solid mainly occurring without a catalyst. It should be mentioned that these are general classes of reactions, but of course, there exist many more in such a complex reaction mixture. Furthermore, some similar compounds were found in the presence of various catalysts but with different concentrations, although some were produced only by specific catalysts.

In **paper I**, it has been observed that HMF and levoglucosan are the most reactive compounds in the simulated pyrolysis oil. The reactions of HMF led to the formation of many furanic intermediates and even crosslinking with other oxygenated groups such as sugar and benzaldehyde/guaiacol derivatives. Melezitose and HMP confirm the occurrence of such reactions (Scheme 2). This is in line with the reports in earlier works on potential cross-polymerization reactions between furan, sugars, and phenols [42,43]. Also, according to Scheme

2, FME, and BMF were probably produced from HMF via possible condensation reactions, giving higher concentrations in the presence of Re/Al_2O_3 catalyst compared to the other catalysts. On the other hand, HMF can undergo hydrogenation to form light hydrotreated furans such as MF, MFA, and DMF, among which MF with high reactivity was predominant using Re/Al_2O_3, and Pt/Al_2O_3. However, for the Pd/Al_2O_3 catalyst, and particularly with its higher loadings (3.9wt%), the formation of stable DMF was the dominant path, along with hydrogenation of the furan ring, formed FAT. However, in the presence of $NiMo/Al_2O_3$ and Rh/Al_2O_3, a variety of furanic compounds containing both reactive and stable furans with DMF as the main compound were observed. Another possible reaction pathway for HMF was its furan ring opening reaction to yield LA as an intermediate, followed by hydrogenation and reactions with alcohol and ketone to generate light ethers such as DD, and ODT as well as heavy oligomers. Although only a trace amount of such ethers was formed in all catalytic experiments using the various catalysts.

Benzaldehyde underwent both hydrogenation, deoxygenation, and condensation reactions to yield toluene as well as benzyl alcohol which can also react with acetic acid to produce an ester (APE). APE, an ester also produced via condensation reactions in all catalytic experiments with higher yield using Pd/Al_2O_3, and Rh/Al_2O_3. The hydrogenation of benzaldehyde that formed benzyl alcohol was the first step in the deoxygenation path and it was followed by HDO to form toluene and/or benzene. Benzyl alcohol was obtained over all catalysts and reached the highest yield using Pd/Al_2O_3 and Rh/Al_2O_3. Although, toluene was only produced in the presence of Pd/Al_2O_3 and $NiMo/Al_2O_3$ and benzene was the deoxygenated compound from Rh/Al_2O_3. Benzoic acid derived from benzaldehyde dehydrogenation was formed mainly when $NiMo/Al_2O_3$ catalyst was used.

Apart from the contribution of acetic acid or its intermediates, in generating esters with alcohol, it is also possible that acetic acid or its intermediates react with phenol, produced from guaiacol hydrogenation, to yield the relevant ester FPE. Also, acetic acid could be hydrogenated into acetone [74] and undergo self-aldol condensation [75] and subsequent reactions to generate heavy soluble oligomers [75].

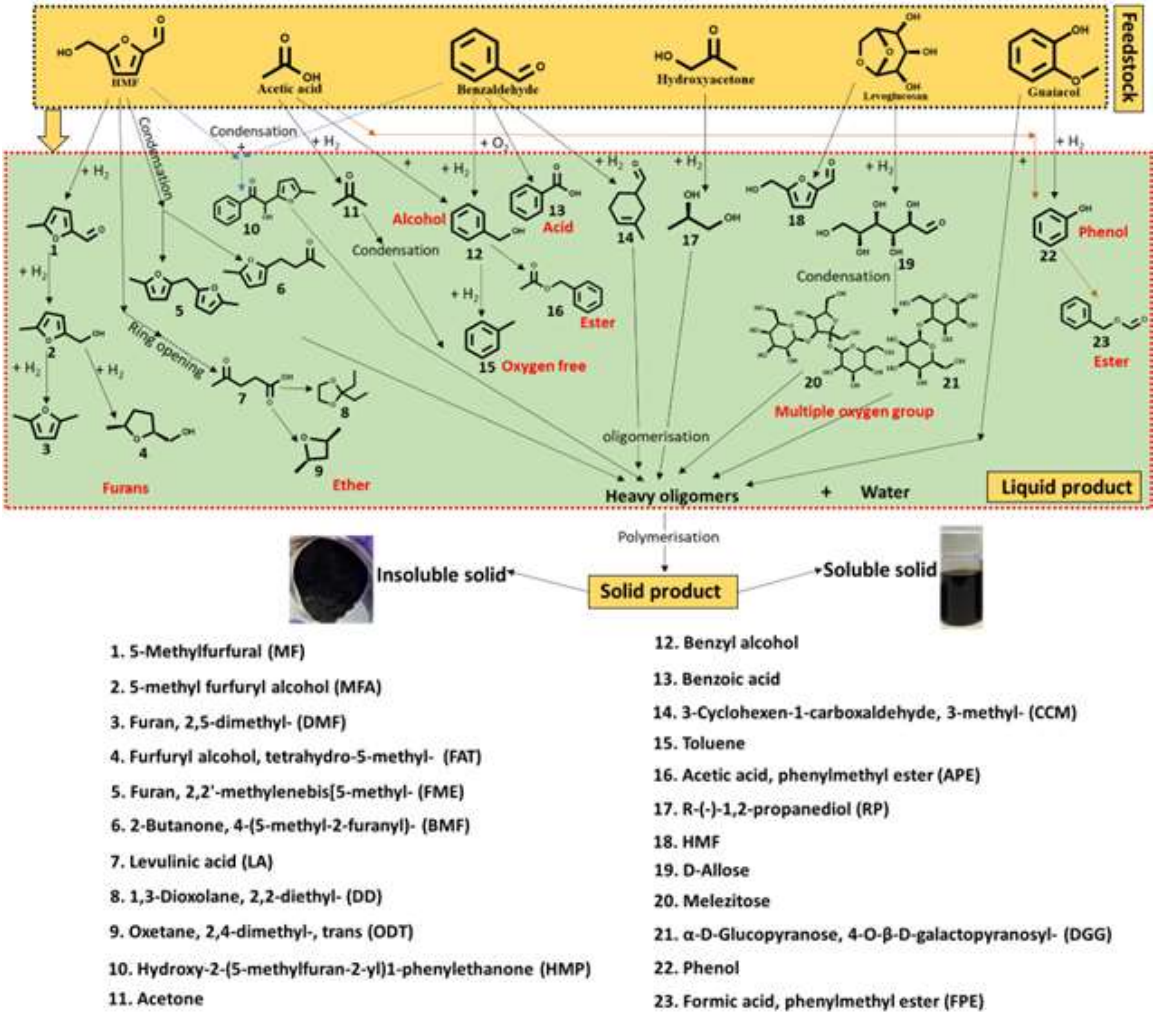

Scheme 2. Reaction pathways proposed for the catalytic mild hydrotreatment of simulated pyrolysis oil at 180°C. Reactions are suggested in accordance with the products identified by GC/MS, including trace compounds and their formation.

Hydroxyacetone can be hydrogenated into alcohol at mild condition [46] as RP was detected as a product, particularly over Pd/Al_2O_3. Furthermore, hydroxyacetone tends to dimerize with other reactive intermediates and proceed with oligomerization reactions. Indeed, hydroxyacetone contributes to hydrogenation reactions to yield relevant alcohols as well as condensation and thus oligomerization reactions [70]. The complexity of the liquid product mixture makes the explanation of further possibilities regarding hydroxyacetone difficult.

Levoglucosan is also found to be very reactive due to its conversion into different products, indicating the possibilities for various reaction pathways. It could convert to HMF via dehydration and yield corresponding intermediates and products. Furthermore, D-allose formed from the sugar ring-opening reaction can contribute to oligomerization reactions. Comparing

all applied catalysts, the yields of these multiple oxygenated compounds derived from condensation of sugar derivatives were higher in the presence of Rh/Al_2O_3, Pd/Al_2O_3, and Pt/Al_2O_3 catalysts (Figure 16). This confirms their inhibitory effect on the further conversion of such condensates (detectable by GC) into heavy oligomers (undetectable by GC) and then polymers/solids.

In the presence of all catalysts tested, guaiacol showed low activity at mild conditions according to its low conversion and probable intermediates. According to GC/MS results, a trace of light phenolic compounds was detected only when Re/Al_2O_3, Pd/Al_2O_3, and Pt/Al_2O_3 were applied. Therefore, it seems guaiacol mostly converted to heavy compounds that were not detectable by GC/MS.

4.3 Catalyst characterization

The elemental composition and textural properties of the alumina-supported catalysts applied in **papers I** and **II** were determined, as depicted in Table 4. The metal loadings (aimed for 2%) are 1.8, 1.7, 1.8, and 1.9 respectively corresponding to Pd, Pt, Rh, and Re. Whereas for $NiMo/Al_2O_3$ catalyst higher loadings were used, due to that these metals likely have a lower activity (3.6 wt% Ni and 13.2 wt% Mo). According to the BET results for the monometallic catalysts, after the metal impregnation, the specific surface areas for all catalysts were slightly decreased from 192.3 m^2g^{-1} for alumina to 181.4 – 191.0 m^2g^{-1}. However, for $NiMo/Al_2O_3$, due to its significantly higher loading of metals, the surface area and pore volume decrease was more pronounced.

Table 4. Textural properties of various catalysts, and their loadings determined by ICP analysis

Sample	S_{BET} [a] (m^2/g)	V_p [b] (cm^3/g)	Metal loading [c] (wt%)	
ɤ-Al_2O_3	192.3	0.48	-	
2 wt% Pd/ɤ-Al_2O_3	181.4	0.46	1.8	
2 wt% Pt/ɤ-Al_2O_3	183.6	0.46	1.7	
2 wt% Rh/ɤ-Al_2O_3	182.2	0.45	1.8	
2 wt% Re/ɤ-Al_2O_3	183.4	0.46	1.9	
$NiMo/ɤ-Al_2O_3$	137.4	0.33	Ni	3.6
			Mo	13.2

[a] Calculated by the BET method

[b] Pore volume

[c] Metal loadings determined by ICP-SFMS

The XRD patterns of the calcined catalysts and ɤ-alumina are presented in Figure 19. All diffraction peaks corresponding to ɤ-alumina (2Θ of 37, 39, 46, and 67°) appeared for all catalysts [76,77]. There were no diffraction peaks detected related to Re/Al_2O_3 and Rh/Al_2O_3, indicating a lower crystallinity of the metal phases in these catalysts, due to high dispersion of these metals and/or too low loading of them. The Pt/Al_2O_3 catalyst had two characteristic peaks at 40.5 and 82°, showing the presence of (111) and (311) planes of Pt [78]. In the case of Pd/Al_2O_3, only a small peak at 34° was seen, indicating PdO [79]. Regarding the $NiMo/Al_2O_3$ catalyst, no relevant peak for Ni and two peaks at 23.5° and 26.7° were visible, which corresponded to the MoO_3 phase [76].

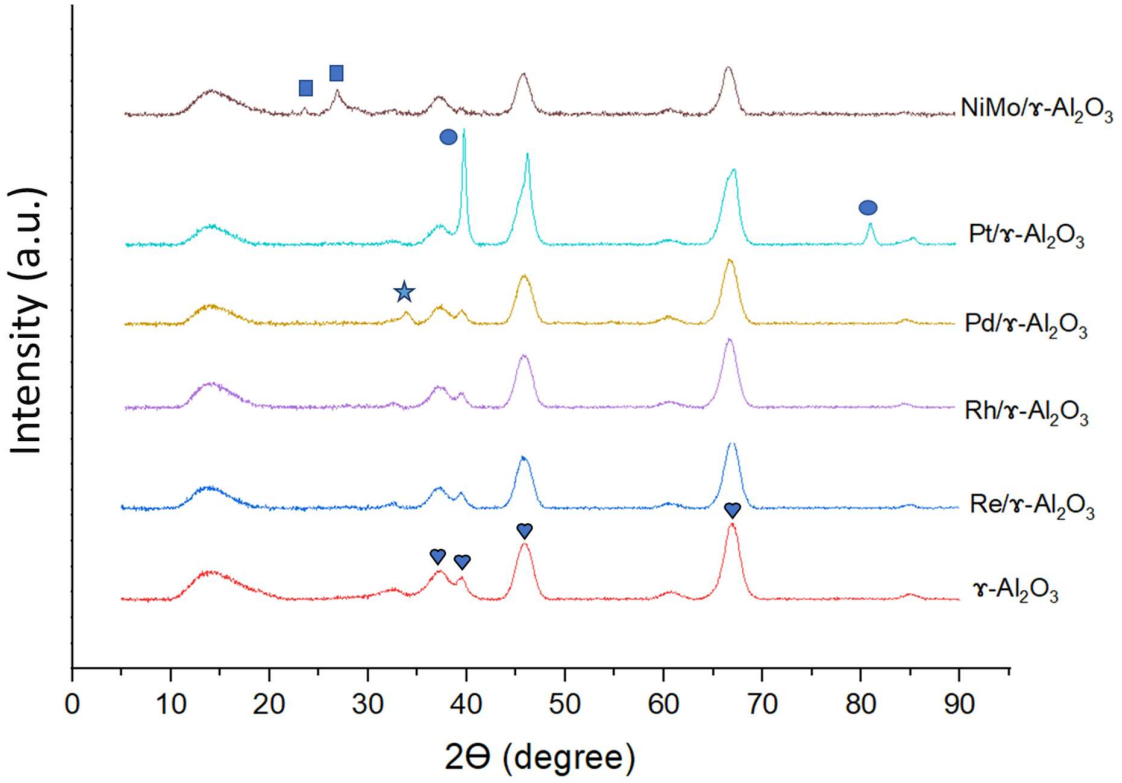

Figure 19. XRD patterns of the catalysts employed.

5 Conclusions

This work involves studies on stabilization of simulated pyrolysis oil by analyzing multiple parameters and utilizing different techniques to gain a deeper understanding of the behavior of pyrolysis oil during mild hydrotreatment.

The effect of reaction conditions (temperature and heating up process) as well as simulated pyrolysis oil composition in thermal and catalytic hydrotreatment using $NiMo/Al_2O_3$ was examined in the first study. Our results indicated that the $NiMo/Al_2O_3$ catalyst positively changed the course of reaction and product distribution compared to in the absence of the catalyst. In the presence of the catalyst a good stabilization efficiency with higher selectivity towards stable oxygenates and HDO reactions was obtained by increasing the reaction temperature from 180 to 300°C. Hydrogenation, esterification, dehydration, hydrocracking, and particularly HDO were the dominant reactions at 300°C while undesirable condensation, oligomerization, and polymerization, and solid yield were drastically reduced. However, in the absence of the catalyst, undesired reaction paths were more favored at elevated temperatures mainly due to the consumption of furans by ring-opening reactions. Solid formation was alleviated with catalyst and reached a minimum yield of 5.7 wt% at 250°C which was four times lower compared to the corresponding catalyst-free experiment. The composition of soluble and insoluble solids obtained from DMSO extraction were determined via NMR, MALDI, and elemental analysis. By increasing the temperature, the yield of soluble solid decreased and its composition changed from macromolecule structures rich in sugar derivatives into aliphatic compounds with lower molecular weight. In the case of insoluble solid with the catalyst, fully developed char was only found at elevated temperatures. Evaluation of the effect of the heating up process to 180°C, in the presence and absence of the catalyst, brought surprising results. Polymerization and thus solid formation initiated only with the catalyst, where the soluble solid contained sugars, and aliphatic compounds and a trace of insoluble solids was not fully developed char. However, the catalyst promoted the rate of hydrogenation simultaneously during heating process. But without the catalyst, the rate of condensation and oligomerization was higher than polymerization causing no solids to be obtained after only heating. However, a considerable increase in solid formation without the catalyst followed by prolonging the reaction time. In the catalytic experiments using the $NiMo/Al_2O_3$ catalyst at 180°C, when HMF and particularly levoglucosan was eliminated from the feed mixture, the most promising result in terms of a higher degree of hydrogenation, and the lowest condensation, polymerization, and

solid product formation was obtained. More importantly, without the catalyst, when HMF was removed a minimum solid among all experiments with and without catalyst was formed indicating the decisive role furans have for solid formation, originated from their tendency to cross-polymerize with other reactive compounds/intermediates. Alongside the solid quantity, they also affected the composition of the solid product favoring formation of more insoluble solids with higher molecular weight. Furthermore, promoting, and inhibitory effects of some compounds on the conversion of others were found. This included the inhibitory effect of sugar on the conversion of benzaldehyde, as well as the promoting effect of HMF on hydroxyacetone conversion and vice versa that were found during mild hydrotreatment.

The effect of different metal sites (Pt, Pd, Rh, Re, and NiMo) over alumina on the stabilization of the simulated pyrolysis oil was explored in the second study. Pd was found to be most effective in terms of both quantity and quality of desired products. It provided the highest conversion of pyrolysis oil compounds to produce a colourless liquid product with the highest yield (~ 66 wt%) containing oxygen-free (toluene) and stabilized oxygenated compounds (hydrogenated furan, esters, and alcohols) with the lowest degree of polymerization and solid formation (3.3 wt%). Rh was also active to selectively convert reactive oxygenates to more stable light compounds, giving a slightly lower yield of liquid and higher yield of solid compared to Pd. Similarly, NiMo showed good performance for stabilization of oxygenates, but not for furans and acids, and was highlighted due to the fact that it attains the highest degree of deoxygenation. The poorest result was observed using Re that gave the lowest yield of liquid product that consisted mainly of heavy oligomers and no deoxygenated light compounds. Re also showed the highest degree of polymerization and carbon loss as solid product. It was also found that only the solid products formed in the catalytic experiments using Pd and Rh were rich in soluble solids. A comparison was made between different Pd loadings over alumina and interestingly lower metal loading was more effective in reducing solid product, however, a higher Pd loading slightly assisted the hydrogenation reactions.

6 Future work

It was found that Pd/Al_2O_3 had a good catalytic activity in stabilizing sugar and furan derivatives, which are the main challenging compounds causing solid formation during mild hydrotreatment. It is therefore, of interest to test and evaluate the effect of such catalysts in stabilization of a real pyrolysis oil at mild conditions to be able to follow subsequent deep HDO over the stabilized oil. In addition, the characterization of the solid product from hydrotreatment of a real pyrolysis oil along with evaluating the effect of reaction parameters (temperature, pressure, time, heating up process) will be interesting to explore. Moreover, the utilization of other methods to stabilize the pyrolysis oil prior to hydrodeoxygenation is also another interesting area for upcoming work in which the reactive compounds in real pyrolysis oil will be removed or converted before further hydroprocessing.

7 References

1 *Total Greenh. Gas Emiss. Trends Proj. Eur. Eur. Environ. Agency*, 2022.

2 *https//www.iea.org/data-and-statistics/charts/biofuel-production-by-country-region-and-fuel-type-2016-2022 (accessed by 20.02.2023)*.

3 *https//www.mordorintelligence.com/industry-reports/europe-biofuel-market (accessed by 20.02.2023)*.

4 H. A. Alalwan, A. H. Alminshid and H. A. S. Aljaafari, *Renew. Energy Focus*, 2019, **28**, 127–139.

5 A. de Rezende Pinho, M. B. B. de Almeida, F. L. Mendes, L. C. Casavechia, M. S. Talmadge, C. M. Kinchin and H. L. Chum, *Fuel*, 2017, **188**, 462–473.

6 R. Sims, M. Taylor, J. Saddler and W. Mobee, *From 1st- to 2nd Gener. Biofuel Technol. An Overv. Curr. Ind. RD&D Act.*, 2008, IEA.

7 P. Moodley, *Sustain. Biofuels*, 2021, 1–20.

8 W. Yin, H. Gu, M. B. Figueirêdo, S. Xia, R. H. Venderbosch and H. J. Heeres, *Fuel Process. Technol.*, 2021, **219**, 106846.

9 Y. Han, M. Gholizadeh, C. C. Tran, S. Kaliaguine, C. Z. Li, M. Olarte and M. Garcia-Perez, *Fuel Process. Technol.*, 2019, **195**, 106140.

10 X. Hu, Z. Zhang, M. Gholizadeh, S. Zhang, C. H. Lam, Z. Xiong and Y. Wang, *Energy & Fuels*, 2020, **34**, 7863–7914.

11 D.-C. Lv, K. Jiang, K. Li, Y.-Q. Liu, D. Wang and Y.-Y. Ye, *Biomass and Bioenergy*, 2022, **159**, 106425.

12 K. Routray, K. J. Barnett and G. W. Huber, *Energy Technol.*, 2017, **5**, 80–93.

13 K. L. Hew, A. M. Tamidi, S. Yusup, K. T. Lee and M. M. Ahmad, *Bioresour. Technol.*, 2010, **101**, 8855–8858.

14 D. C. Elliott and E. G. Baker, 1989, US Patent 4795841.

15 R. H. Venderbosch, A. R. Ardiyanti, J. Wildschut, A. Oasmaa and H. J. Heeres, *J. Chem. Technol. Biotechnol.*, 2010, **85**, 674–686.

16 J. Chen, S. Wang, L. Lu, X. Zhang and Y. Liu, *Fuel Process. Technol.*, 2018, **179**, 135–142.

17 C. Boscagli, K. Raffelt, T. A. Zevaco, W. Olbrich, T. N. Otto, J. Sauer and J.-D. Grunwaldt, *Biomass and Bioenergy*, 2015, **83**, 525–538.

18 M. V Olarte, A. H. Zacher, A. B. Padmaperuma, S. D. Burton, H. M. Job, T. L. Lemmon, M. S. Swita, L. J. Rotness, G. N. Neuenschwander and J. G. Frye, *Top. Catal.*, 2016, **59**, 55–64.

19 W. Yin, A. Kloekhorst, R. H. Venderbosch, M. V Bykova, S. A. Khromova, V. A. Yakovlev and H. J. Heeres, *Catal. Sci. Technol.*, 2016, **6**, 5899–5915.

20 T. M. H. Dabros, M. Z. Stummann, M. Høj, P. A. Jensen, J.-D. Grunwaldt, J. Gabrielsen, P. M. Mortensen and A. D. Jensen, *Prog. Energy Combust. Sci.*, 2018, **68**, 268.

21 E. C. Okoroigwe, Z. Li, S. Kelkar, C. Saffron and S. Onyegegbu, *J. Energy South. Africa* , 2015, 26, 33–41.

22 M. Asadieraghi, W. M. Ashri Wan Daud and H. F. Abbas, *RSC Adv.*, 2015, **5**, 22234–22255.

23 C. Liu, H. Wang, A. M. Karim, J. Sun and Y. Wang, *Chem. Soc. Rev.*, 2014, **43**, 7594–7623.

24 J. Wildschut, F. H. Mahfud, R. H. Venderbosch and H. J. Heeres, *Ind. Eng. Chem. Res.*, 2009, **48**, 10324.

25 H. Shafaghat, I.-G. Lee, J. Jae, S.-C. Jung and Y.-K. Park, *Chem. Eng. J.*, 2019, **377**, 119986.

26 H. Shafaghat, M. Linderberg, T. Janosik, M. Hedberg, H. Wiinikka, L. Sandström and A.-C. Johansson, *Energy & Fuels*, 2021, **36**, 450–462.

27 R. Pujro, J. R. García, M. Bertero, M. Falco and U. Sedran, *Energy & Fuels*, 2021, **35**, 16943–16964.

28 P. Yan, J. Mensah, M. Drewery, E. Kennedy, T. Maschmeyer and M. Stockenhuber, *Appl. Catal. B Environ.*, 2021, **281**, 119470.

29 S. Oh, H. Hwang, H. S. Choi and J. W. Choi, *Fuel*, 2015, **153**, 535–543.

30 C. Zhang, J. Qi, J. Xing, S.-F. Tang, L. Song, Y. Sun, C. Zhang, H. Xin and X. Li, *RSC Adv.*, 2016, **6**, 104398–104406.

31 G. Kim, J. Seo, J.-W. Choi, J. Jae, J.-M. Ha, D. J. Suh, K.-Y. Lee, J.-K. Jeon and J.-K. Kim, *Catal. Today*, 2018, **303**, 130–135.

32 S. Jin, Z. Xiao, C. Li, X. Chen, L. Wang, J. Xing, W. Li and C. Liang, *Catal. Today*, 2014, **234**, 125.

33 K. Kohli, R. Prajapati, S. K. Maity and B. K. Sharma, *Energies*, 2020, **13**, 4967.

34 S. Kadarwati, X. Hu, R. Gunawan, R. Westerhof, M. Gholizadeh, M. D. M. Hasan and C.-Z. Li, *Fuel Process. Technol.*, 2017, **155**, 261–268.

35 J. Payormhorm, K. Kangvansaichol, P. Reubroycharoen, P. Kuchonthara and N. Hinchiranan, *Bioresour. Technol.*, 2013, **139**, 128.

36 C. R. Lee, J. S. Yoon, Y.-W. Suh, J.-W. Choi, J.-M. Ha, D. J. Suh and Y.-K. Park, *Catal. Commun.*, 2012, **17**, 54–58.

37 Z. He and X. Wang, *Front. Chem. Sci. Eng.*, 2014, **8**, 369–377.

38 M. S. Zanuttini, M. A. Peralta and C. A. Querini, *Ind. Eng. Chem. Res.*, 2015, **54**, 4929–4939.

39 T. Nimmanwudipong, R. C. Runnebaum, K. Tay, D. E. Block and B. C. Gates, *Catal. Letters*, 2011, **141**, 1072–1078.

40 S. Bhogeswararao and D. Srinivas, *J. Catal.*, 2015, **327**, 65–77.

41 J. Lee, Y. Xu and G. W. Huber, *Appl. Catal. B Environ.*, 2013, **140**–**141**, 98–107.

42 Q. Xu, K. Sun, Y. Shao, C. Zhang, S. Zhang, L. Zhang, P. Jia, S. Wang, Q. Liu and X. Hu, *Bioresour. Technol. Reports*, 2019, **8**, 100324.

43 Q. Xu, L. Zhang, K. Sun, Y. Shao, H. Tian, S. Zhang, Q. Liu, G. Hu, S. Wang and X. Hu, *J. Energy Inst.*, 2020, **93**, 1678–1689.

44 X. Hu, Y. Wang, D. Mourant, R. Gunawan, C. Lievens, W. Chaiwat, M. Gholizadeh, L. Wu, X. Li and C.-Z. Li, *AIChE J.*, 2013, **59**, 888–900.

45 H. Wan, R. V Chaudhari and B. Subramaniam, *Energy & Fuels*, 2013, **27**, 487–493.

46 D. Han, W. Yin, A. Arslan, T. Liu, Y. Zheng and S. Xia, *Catalysts*, 2020, **10**, 402.

47 K. Sun, L. Zhang, Q. Xu, Z. Zhang, Y. Shao, D. Dong, G. Gao, Q. Liu, S. Wang and X. Hu, *Renew. Energy*, 2020, **154**, 517–531.

48 X. Hu, K. Nango, L. Bao, T. Li, M. D. M. Hasan and C.-Z. Li, *Green Chem.*, 2019, **21**, 1128–1140.

49 R. Gunawan, X. Li, A. Larcher, X. Hu, D. Mourant, W. Chaiwat, H. Wu and C.-Z. Li, *Fuel*, 2012, **95**, 146–151.

50 S. Li, S. Zhang, Z. Feng and Y. Yan, *Environ. Prog. Sustain. Energy*, 2015, **34**, 240–247.

51 S. Shao, H. Zhang, R. Xiao and D. Shen, *Energy Technol.*, 2017, **5**, 111–118.

52 S. Kadarwati, S. Oudenhoven, M. Schagen, X. Hu, M. Garcia-Perez, S. Kersten, C.-Z. Li and R. Westerhof, *J. Anal. Appl. Pyrolysis*, 2016, **118**, 136–143.

53 I. Speciale, A. Notaro, P. Garcia-Vello, F. Di Lorenzo, S. Armiento, A. Molinaro, R. Marchetti, A. Silipo and C. De Castro, *Carbohydr. Polym.*, 2022, **277**, 118885.

54 Y. Yu, Y. W. Chua and H. Wu, *Energy & Fuels*, 2016, **30**, 4145–4149.

55 W. A. Bubb, *Concepts Magn. Reson.*, 2003, **19A**, 1–19.

56 N. Priharto, F. Ronsse, W. Prins, R. Carleer and H. J. Heeres, *Fuel Process. Technol.*, 2020, **206**, 106466.

57 H. Ben and A. J. Ragauskas, *Energy & Fuels*, 2011, **25**, 5791–5801.

58 W. Yin, M. V. A. (Bykova), R. H. Venderbosch, V. A. Yakovlev and H. J. Heeres, *Energies*, 2020, **13**, 285.

59 X. Zhang, H. Ma, S. Wu, W. Jiang, W. Wei and M. Lei, *Fuel*, 2019, **242**, 587–595.

60 M. Guisnet and P. Magnoux, *Appl. Catal. A Gen.*, 2001, **212**, 83–96.

61 A. Achour, D. Bernin, D. Creaser and L. Olsson, *Chem. Eng. J.*, 2023, **453**, 139829.

62 S. Shao, H. Zhang, R. Xiao, X. Li and Y. Cai, *J. Anal. Appl. Pyrolysis*, 2017, **127**, 258–268.

63 C. Z. Li, R. Gunawan, M. Gholizadeh and W. Chaiwat, 2015, US patent

WO2014015380A1.

64 M. Gholizadeh, R. Gunawan, X. Hu, S. Kadarwati, R. Westerhof, W. Chaiwat, M. M. Hasan and C.-Z. Li, *Fuel Process. Technol.*, 2016, **150**, 132–140.

65 A. D. K. Deshan, L. Atanda, L. Moghaddam, D. W. Rackemann, J. Beltramini and W. O. S. Doherty, *Front. Chem.*, 2020, **8**, 659.

66 D. W. Ball, J. W. Hill and R. J. Scott, in *TThe Basics of General, Organic, and Biological Chemistry; Saylor*, 2011.

67 X. Hu and C.-Z. Li, *Green Chem.*, 2011, **13**, 1676.

68 Y. Li, C. Zhang, Y. Liu, S. Tang, G. Chen, R. Zhang and X. Tang, *Fuel*, 2017, **189**, 23–31.

69 J. Wildschut, J. Arentz, C. B. Rasrendra, R. H. Venderbosch and H. J. Heeres, *Environ. Prog. Sustain. Energy*, 2009, **28**, 450–460.

70 E. Nejadmoghadam, A. Achour, P. S. Rezaei, M. A. Salam, P. Arora, O. Öhrman, D. Creaser and L. Olsson, *submitted.*

71 R. J. French, J. Stunkel, S. Black, M. Myers, M. M. Yung and K. Iisa, *Energy & Fuels*, 2014, **28**, 3086–3095.

72 A. Eschenbacher, A. Saraeian, B. H. Shanks, P. A. Jensen, C. Li, J. Ø. Duus, A. B. Hansen, U. V. Mentzel, U. B. Henriksen and J. Ahrenfeldt, *Sustain. Energy Fuels*, 2020, **4**, 1991–2008.

73 Y.-C. Lin, C.-L. Li, H.-P. Wan, H.-T. Lee and C.-F. Liu, *Energy Fuels*, 2011, **25**, 890.

74 S. F. Zaman, H. S. Bamufleh, A. Al-Zahrani, M. R. A. Rafiqui, Y. A. Alhamed and L. Petrov, *Compt. Rend. Acad. bulg. Sci.*, **71**, 2018.

75 W. Zhang, Y. Zhang, L. Zhao and W. Wei, *Energy & Fuels*, 2010, **24**, 2052–2059.

76 C. Muangsuwan, W. Kriprasertkul, S. Ratchahat, C.-G. Liu, P. Posoknistakul, N. Laosiripojana and C. Sakdaronnarong, *ACS Omega*, 2021, **6**, 2999–3016.

77 M. A. Salam, Y. W. Cheah, P. H. Ho, D. Bernin, A. Achour, E. Nejadmoghadam, O. Öhrman, P. Arora, L. Olsson and D. Creaser, *Chem. Eng. J.*, 2022, **442**, 136216.

78 R. Garidzirai, P. Modisha, I. Shuro, J. Visagie, P. van Helden and D. Bessarabov,

Catalysts, 2021, 11.

79 C. A. Teles, R. C. Rabelo-Neto, J. R. de Lima, L. V Mattos, D. E. Resasco and F. B. Noronha, *Catal. Letters*, 2016, **146**, 1848–1857.